

**Recognition of peptide and protein phosphorylation
and
Inhibition of melanoma inhibitory activity (MIA) protein**

Dissertation

zur Erlangung des Doktorgrades der Naturwissenschaften

(Dr. rer. nat.)

**an der Fakultät für Chemie und Pharmazie
der Universität Regensburg**



**vorgelegt von
Alexander Riechers
aus Göttingen**

2010

The thesis was submitted on: March 18th, 2010

The colloquium took place on: May 4th, 2010

Chairman:

Prof. Dr. H. A. Wagenknecht

1st Referee:

Prof. Dr. B. König

2nd Referee:

Prof. Dr. A. K. Bosserhoff

3rd Referee:

Prof. Dr. O. S. Wolfbeis

**If you're not part of the solution,
you're part of the precipitate.**

- Henry J. Tillman

The experimental part of this work was carried out from October 2007 to January 2010 at the Institute for Organic Chemistry at the University of Regensburg and at the Institute of Pathology of the University of Regensburg under the supervision of Prof. Dr. B. König.

Completing a PhD thesis is never possible without a lot of help, so I extend my sincerest gratitude to:

First and foremost, I thank Prof. Dr. B. König for the interesting tasks, his interest in the progress of this work as well as his guidance and support. Furthermore, I have to thank him for his unbelievable trust in letting me initiate and cancel projects and cooperations as I saw fit. It was a great pleasure to be able to work so freely in a way I have not witnessed in any other working group.

I also thank Prof. Dr. A. K. Bosserhoff for letting another chemist join the Institute of Pathology. Her enthusiasm and critical assessment of ideas contributed significantly to the studies of the MIA inhibitors.

I have to thank A. Grauer, C. Woinaroschy, F. Schmidt, B. Gruber, J. Schmidt (both of them!), S. Wallner and E. Wacker for all the laughs and the good time in the lab. I further thank G. Dirscherl and S. Kiewitz for advice about the intricacies of solid-phase peptide synthesis and A. Späth for discussions about fluorescence titrations.

Special thanks go to J. Schmidt for setting up a great cooperation with me between the Institutes of Pathology and Organic Chemistry and teaching me so much about molecular biology. In the lab, being two chemists in a group of biologists was certainly never boring.

Additionally, I have to thank S. Wallner and S. Kaufmann for help with the PCRs and histological analyses. I also would like to thank T. Amann and T. Spruss for all the great discussions and for help with the mouse experiments.

Further thanks go to R. Vasold and S. Strauss for the HPLC measurements and J. Kirmeier for the MS analyses.

Finally, my thanks go to my parents and the rest of my family. Without their support (mentally and financially!) this work would not have been possible.

I, Alexander Riechers, solemnly declare to have completed this work without any aid or help of any kind not mentioned in this thesis.

Regensburg,.....

meinen Eltern

Content

1. Recognition of peptide and protein phosphorylation.....	1
1.1 Using ditopic receptors for the recognition of phosphorylated peptides	2
1.1.1 Introduction	2
1.1.2 Results of the binding studies.....	5
1.1.3 Discussion of the binding studies.....	9
1.1.4 Conclusion.....	10
1.1.5 Materials and Methods	11
1.2 Detection of protein phosphorylation on SDS-PAGE.....	19
1.2.1 Introduction	19
1.2.2 Results and Discussion of the phosphostaining	20
1.2.3 Conclusion.....	24
1.2.4 Materials and Methods	24
2. Inhibition of melanoma inhibitory activity (MIA) protein.....	26
2.1 Development of a screening assay for inhibitors of melanoma inhibitory activity (MIA) protein.....	27
2.1.1 Introduction	27
2.1.2 Results of the HTFP assay studies	28
2.1.3 Discussion of the HTFP assay studies.....	33
2.1.4 Materials and Methods	35
2.2 Dissociation of functionally active MIA dimers by dodecapeptide AR71 strongly reduces formation of metastases in malignant melanoma.....	38
2.2.1 Introduction	38
2.2.2 Results of the inhibition studies	39
2.2.3 Discussion of the inhibition studies	47
2.2.4 Materials and Methods	49
3. Summary in English and in German.....	55
4. Abbreviations.....	56
5. Publications, patents and award	58
6. Curriculum Vitae	60
7. Literature	61

1. Recognition of peptide and protein phosphorylation

The results presented in this chapter were achieved in collaboration with other scientists. In the work on the ditopic receptors, I have synthesized the labeled phosphorylated peptides and have performed all binding studies towards peptides **3** and **4**. A. Grauer and S. Ritter have synthesized the artificial receptors while B. Sperl and T. Berg have performed the STAT1 and Chk2 related binding studies.

In the work on detecting protein phosphorylation on SDS-PAGE, I have performed the electrophoresis experiments and established the staining technique. F. Schmidt and S. Stadlbauer have synthesized probes **1** and **2**. B. König has been supervising both projects.

The results of this chapter have been published:

Riechers, A., Grauer, A., Ritter, S., Sperl, B., Berg, T., König, B. Binding of phosphorylated peptides and inhibition of their interaction with disease-relevant human proteins by synthetic metal-chelate receptors. *J. Mol. Recognit.* **2009**, (in print).

Riechers, A., Schmidt, F., Stadlbauer, S., König, B. Detection of protein phosphorylation on SDS-PAGE using probes with a phosphate-sensitive emission response. *Bioconj. Chem.* **2009**, *20*, 804 – 807.

1.1 Using ditopic receptors for the recognition of phosphorylated peptides

1.1.1 Introduction

The selective modulation of protein function by small molecules is still a major challenge in medicinal chemistry and molecular biology. Most approaches target the active or allosteric binding sites of enzymes or receptors, which are addressed by ligands acting as agonist or antagonist. Far less explored is the selective inhibition of protein – protein interactions to intercept biological signal transduction. Many of such protein – protein interactions are regulated by phosphorylation of one of the binding partners and are of key importance for the regulation of essential biological processes, such as cell proliferation.^{1, 2}

While an enzyme inhibitor or receptor ligand is accommodated in a well defined binding cleft inducing a pharmacologic response, the specific interaction of two proteins typically involves much larger surface areas and multiple interactions of complementary functional groups and charges. This severely complicates the rational design of inhibitor molecules intercepting specific protein interactions making the screening of compound libraries³ or protein crystal structure based design analyses^{4, 5} necessary to identify inhibitors.

Reversible coordination of metal complexes to charged protein structures provides high affinity under physiological conditions and neutralizes protein surface charges upon binding, which renders them promising tools for the specific inhibition of protein – protein interactions. Although metal chelates have been widely used in molecular recognition,⁶ only few examples of protein function regulation by metal – ligand coordination are known so far.^{7, 8} A particularly suitable target for cationic metal complexes in protein binding are phosphorylated amino acid residues due to their negative charges, low abundance and importance for the regulation of nearly every cellular process.^{9, 10, 11} The binding selectivity and affinity of metal complex binding sites is enhanced if they are combined with functional groups that allow for additional specific interactions with the target peptide sequence. We have recently used such ditopic metal complex based receptors for the discrimination of phosphorylated peptides with nanomolar affinities.¹²

Herein, we report the synthesis of a larger series of metal chelate receptors and their binding affinities in a protein inhibition assay. As model protein targets, we chose the human signal transducer and activator of transcription protein STAT1 and the serine/threonine kinase Chk2. STATs transduce signals from the cell surface to the nucleus¹³ and contain a Src homology

(SH) 2 domain, by which they bind to activated cytokine receptors and growth factor receptors. This binding event is prerequisite to the subsequent phosphorylation of STATs at a conserved tyrosine residue C-terminal of their SH2 domain, which leads to formation of STAT dimers via reciprocal phosphotyrosine-SH2 domain interactions. The so formed STAT dimers translocate to the nucleus, where they regulate gene expression.¹⁴ Since binding of STATs to activated receptors bearing a phosphotyrosine residue is an early step in STAT signaling, small molecules like the complexes presented in this work might potentially be used as inhibitors of STAT activation. The family member STAT1 mediates responses to interferons, and is therefore important for fighting viral and bacterial infections. However, because aberrant interferon-mediated signaling leads to inflammatory diseases, STAT1 is also a likely target for inflammatory disorders.¹⁵ The serine/threonine kinase Chk2 is involved in DNA damage signaling and mediates checkpoint activation and cell cycle arrest upon DNA damage. It carries a forkhead-associated (FHA) domain, which binds to peptide motifs comprising phosphothreonine residues.¹⁶

We have previously reported that bis-zinc(II)-cyclen triazine **18** employed as one of the two binding sites in the synthetic receptors coordinates to phosphorylated amino acids under physiological conditions.¹² With lower affinity, this moiety also binds to histidine residues. Likewise, we found that a zinc(II)-NTA **19** (nitrilotriacetic acid) complex, which represents a truncated EDTA motif can bind carboxylates. The receptors **15** – **17** bear a guanidinium moiety as a second binding site since we expected this motif to also bind to carboxylates. Histidine and aspartic or glutamic acid, respectively, were thus the secondary binding sites in the peptides targeted by our ditopic receptors. We now sought to exploit these binding preferences for the design of the potential inhibitors of binding of STAT1 and Chk2, respectively, to their phosphorylated peptide recognition motifs. A series of synthetic receptors **5** – **17** for peptide binding was prepared, with the receptors differing in their binding sites as well as in the length and nature of the linker connecting both binding sites (see Figure 1).

The peptide sequence (Flu-GpYDKPHVL, **1**) derived from the interferon- γ receptor, which is known to play a critical role for STAT1 activation, was chosen for the determination of STAT binding inhibition by metal chelates.¹⁷ Similarly, the peptide Flu-GHFDpTYLIRR (**2**) which had been described as the optimal ligand of the forkhead-associated (FHA) domain of the serine/threonine kinase Chk2,¹⁸ was selected as a target for our receptors. To prove the respective binding selectivity for imidazole or carboxylate containing amino acid side chains,

we also prepared the two peptides Flu-GpSAAEV-NH₂ (**3**) and Flu-GpSAAHV-NH₂ (**4**) which do not contain functional side chains beside the two targeted residues. Without other functional side chains, they should allow an unambiguous investigation on the influence of the secondary binding site. All target peptides are labeled with carboxyfluorescein to allow the determination of the binding constants by fluorescence emission and fluorescence polarization measurements.

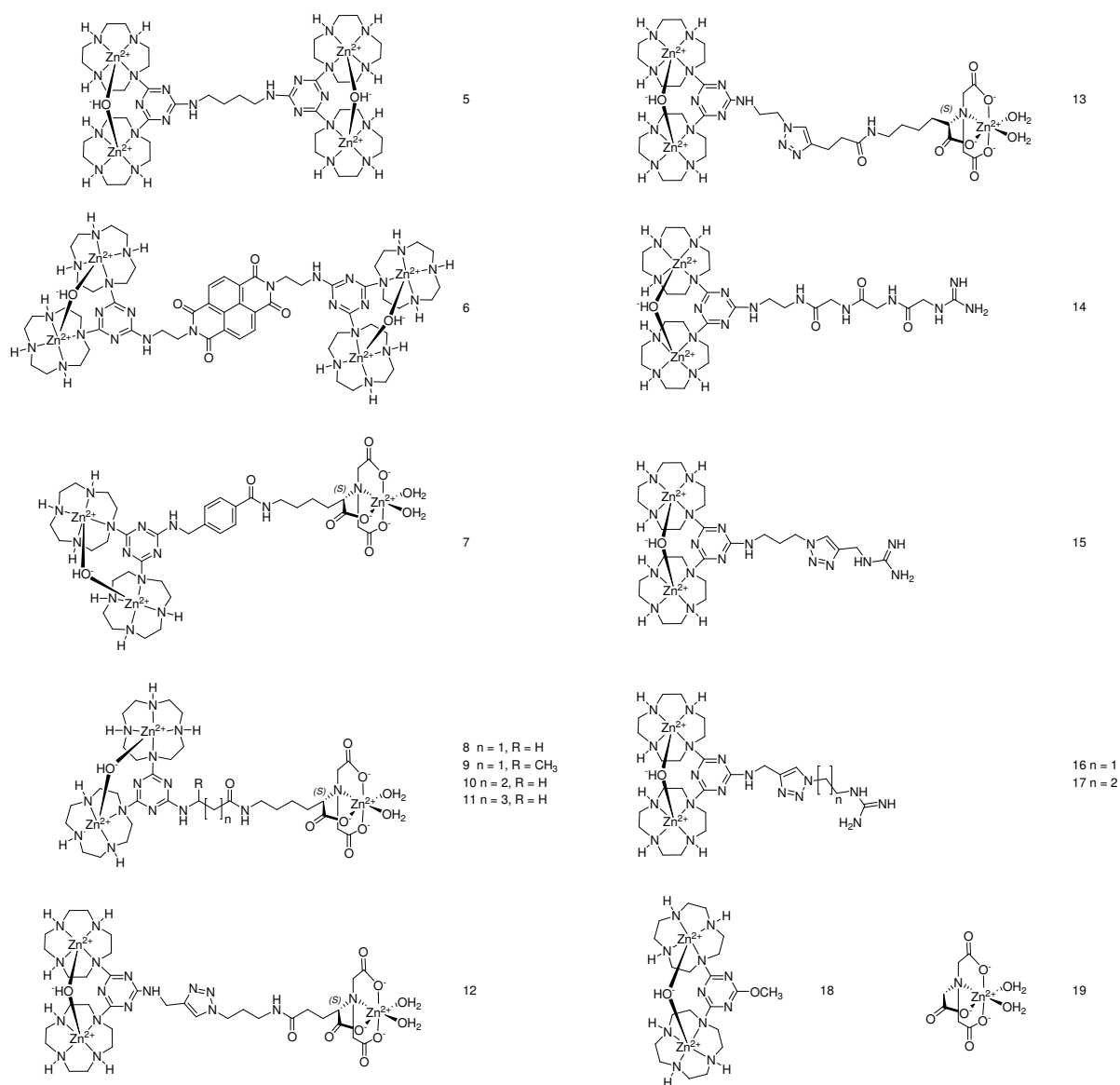


Figure 1. Synthetic receptors **5** - **17** and complexes **18** and **19** representing receptor substructures. Counterions are omitted for clarity.

1.1.2 Results of the binding studies

Binding to peptides **3** and **4**

Fluorescence emission titrations were performed to determine the binding constants of the prepared synthetic receptors to peptides **3** and **4**. The determined affinities were exemplarily verified by fluorescence polarization titrations as an independent method.¹² Binding stoichiometries were determined by Job's plot analysis and were found to be 1:1 in all cases.

As the bis-zinc(II)-cyclen triazine moiety of the receptors **7** – **13** shows a binding affinity for phosphorylated amino acids, and the zinc(II)-NTA can bind to carboxylates, we expected a marked selectivity for peptide **3** over **4**. Table 1 shows that this is indeed the case. Furthermore, the significant increase in binding affinity of the ditopic receptors over the receptor fragments **18** and **19** indicates additive or even cooperative binding of the individual sites to the target peptides.¹⁹

The same binding preference was observed for receptors **14** – **17**. In these cases, the coordination of the guanidinium moiety to the carboxylate side chain is a likely rationale for the selectivity. However, differences in binding affinity to peptides **3** and **4** are less pronounced with these receptors, probably due to the weaker guanidinium – carboxylate interaction if compared to the glutamic acid side chain – zinc(II) –NTA interaction.

With receptors **5** and **6**, the binding affinities are higher for peptide **4** as one bis-zinc(II)-cyclen triazine can coordinate to the phosphorylated serine while the other binds to the imidazole side chain of the histidine. In peptide **3** only the phosphate group is a suitable binding partner for receptors **5** and **6** as bis-zinc(II)-cyclen triazine shows no measurable affinity to carboxylates.¹²

In all cases, we found no marked influence of the length or structure of the linker. This can be explained by the fact that peptides as short as the ones used in this study show no defined secondary structure in solution. Having determined binding affinities and selectivities to model peptides **3** and **4**, we selected the synthetic receptors **8**, **10**, **15**, **16** due to their good solubility, and the reference compound **18** to investigate their ability to interfere with binding between peptides comprising phosphorylated amino acids and their respective protein binding partners, STAT1 and Chk2.

receptor	binding affinity [logK]	
	peptide 4	peptide 3
5	6.5	5.0
6	6.5	4.9
7	5.2	7.5
8	5.1	8.3
9	4.8	8.2
10	5.0	8.4
11	5.0	7.8
12	5.4	8.1
13	5.5	8.1
14	4.8	7.8
15	5.2	7.0
16	4.8	7.7
17	5.0	6.8
18	4.8	4.8
19	< 3	n.d.

Table 1. Binding affinities of receptors **5** – **17** and substructures **18** and **19** to peptides **3** and **4**, reported as logK values ± 0.2 .

Inhibition of peptide 1 – STAT1 interaction

The effect of receptors **8**, **10**, **15**, **16**, and bis-zinc(II)-cyclen triazine **18** on binding between peptide **1** and STAT1 was analyzed by fluorescence polarization (Figure 2). Receptor **18** served as a reference compound for all measurements. Inhibition by **18** should occur at higher concentrations compared to the other receptors as it contains only one binding site.

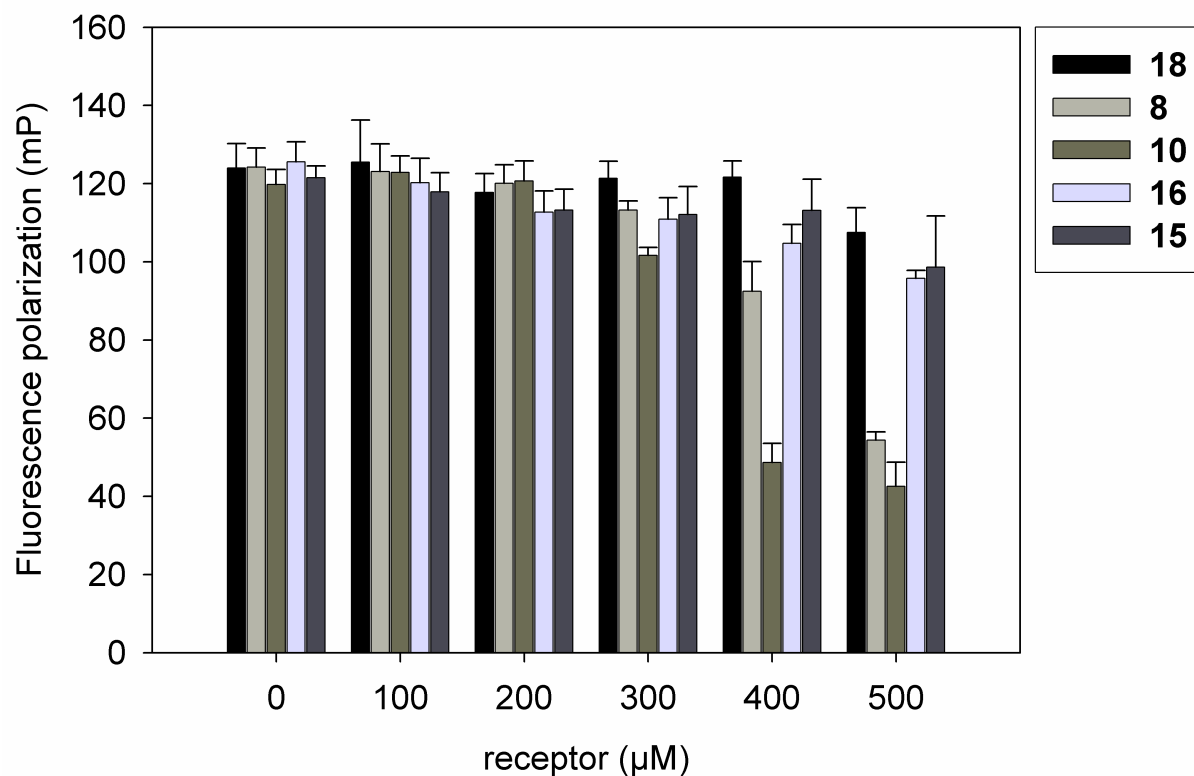


Figure 2. Effect of receptors **8**, **10**, **15**, **16** and the reference compound **18** on fluorescence polarization of peptide **1** in the presence of its natural binding partner STAT1.

The measurements revealed that receptor **10** is significantly more potent than reference compound **18** at concentrations of 300 μM and higher, and that receptor **8** is also significantly more active than **18** at 400 μM and 500 μM . Receptors **15** and **16** are slightly more active than **18**, but the statistical significance of this effect remains to be investigated.

Inhibition of peptide **2** – Chk2 interaction

The inhibition of the interaction of peptide **2** with the FHA domain of Chk2 by receptors **8**, **10**, **15** and **16** was investigated likewise (see Figure 3). The results show that receptors **8** and **10** affect the peptide **2** – Chk2 binding at concentrations at 300 μM and higher. The reference compound **18** inhibits this peptide – protein binding only at a concentration of 500 μM . Again, the ditopic receptors exhibited a higher affinity than the bis-zinc(II)-cyclen triazine **18**. As with the peptide **1** – STAT1 inhibition, the guanidinium-containing receptors **15** and **16** show no significantly stronger inhibitory effect than the reference compound **18**.

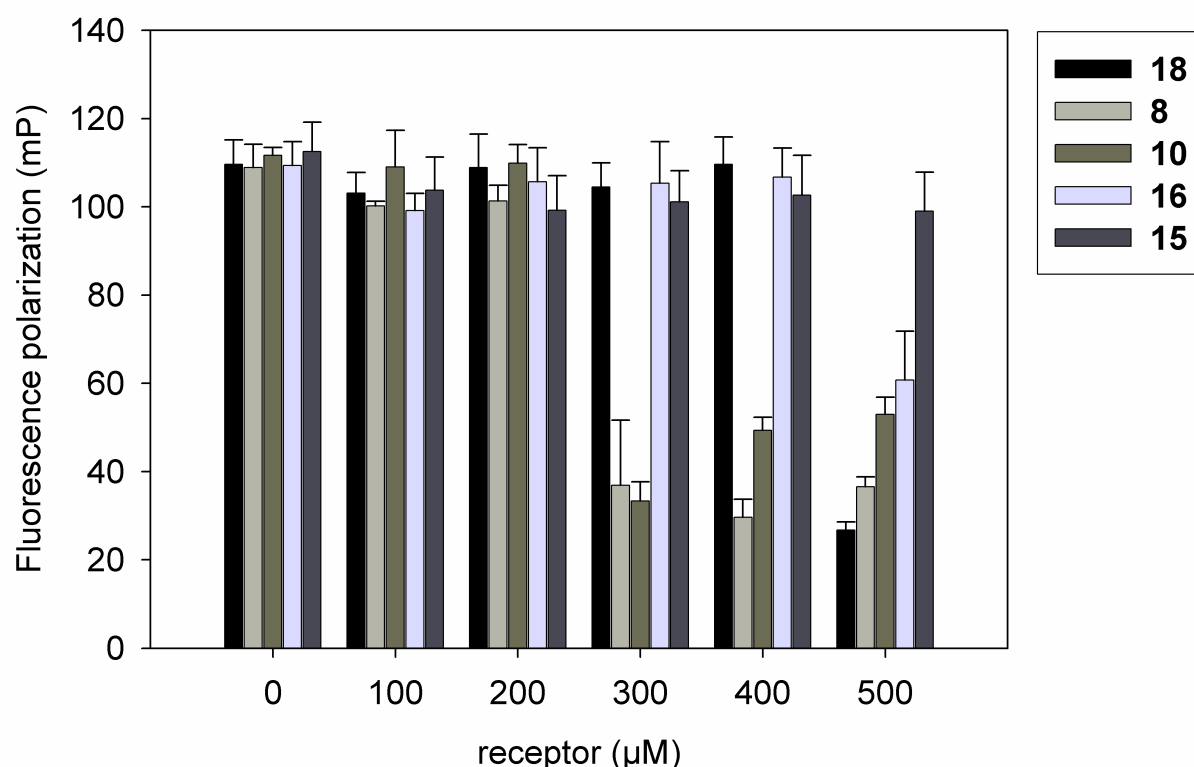


Figure 3. Effect of receptors **8**, **10**, **15**, **16** and the reference compound **18** on fluorescence polarization of peptide **2** in the presence of its natural binding partner, the Chk2 FHA domain.

1.1.3 Discussion of the binding studies

The fluorescence polarization values monitored in both peptide – protein interaction assays, especially in the peptide **2** – Chk2 interaction assay, decrease relatively sharply with increasing concentrations of the most active receptors **8** and **10**. Furthermore, in case of the peptide **2** – Chk2 interaction, fluorescence polarization increases again slightly at higher concentrations of receptors **8** and **10**. This behavior is consistent with the idea that the receptors do not bind to the larger binding partner that is usually targeted in fluorescence polarization assays, but instead bind to the fluorophore-labeled peptide.

Binding of the receptors to the fluorophore-labeled peptides increases the fraction of peptides that are not bound to the respective target protein and rotate rapidly in solution, and thereby decreases fluorescence polarization. However, it can be speculated that this effect can be partially masked by two concomitant, opposing effects that instead *increase* fluorescence polarization. Firstly, in the presence of the artificial receptors, the remaining fluorophore-labeled peptides which are not inactivated by the receptors may bind to their target protein to a higher proportion, which would provide a positive contribution to the overall fluorescence polarization. This model is supported by the decrease in the dissociation constants (K_d -values) of the peptide **2** – Chk2 interaction with decreasing concentrations of peptide **2** (K_d -values of the peptide **2** – Chk2 interaction in the presence of 10 nM, 5 nM, 2.5 nM, and 1 nM peptide **2**: 112 ± 7 nM, 90 ± 11 nM, 99 ± 12 nM, and 71 ± 20 nM). Thus, fluorescence polarization values of fluorophore-labeled peptide **2** in the presence of Chk2 tend to be higher at lower peptide concentrations (Figure 19A). Secondly, binding of the artificial receptors to the fluorophore-labeled peptides increases their molecular weight and decreases their rotational mobility, again providing a positive contribution to fluorescence polarization. In support of this theory, we observed a dose-dependent increase in fluorescence polarization of peptide **2** in the presence of various concentrations of receptors **8** and **10** (Figure 19B). Both effects can be expected to mask low-to-moderate inhibitions obtained at lower concentrations of the artificial receptors, and will only be outweighed under conditions of strong disruption of the peptide – protein interaction, thus providing a rationale for strong changes of fluorescence polarization within a small concentration window of the artificial receptors. The second effect furthermore explains why at receptor concentrations exceeding those required for disruption of the peptide **2** – Chk2 interaction, a slight dose-dependent *increase* in the fluorescence polarization is observed instead of a further decrease (compare fluorescence polarization

values for receptor **10** at 300 μM , 400 μM , and 500 μM ; also compare data for receptor **8** at 400 μM and 500 μM). Consistent with our findings, Hamachi and co-workers had also reported a slight increase in fluorescence anisotropy, which is directly linked to fluorescence polarization, of a phosphorylated peptide designed to bind to the Pin1 WW domain at high concentrations of an effective artificial receptor.²⁰ In addition to that, we have also been successful in using fluorescence polarization for detecting the binding of fluorescein-labeled peptides and synthetic receptors with similar molecular weight.¹² Receptor concentrations exceeding 500 μM could not be tested in our assays due to solubility problems at higher concentrations.

The most active receptors **8** and **10** affect the peptide **1** – STAT1 interaction somewhat less abrupt than the peptide **2** – Chk2 interaction discussed above. It appears conceivable that the effects outlined above do not play an equally significant role for this peptide – protein interaction. Analysis of the K_d -values of the peptide **1** – STAT1 interaction in the presence of 10 nM, 5 nM, 2.5 nM, and 1 nM of peptide **1** did not reveal clear trends in affinity (K_d -values at 10 nM, 5 nM, 2.5 nM and 1 nM of peptide **1**: 141 ± 4 nM, 119 ± 10 nM, 114 ± 8 nM, and 136 ± 54 nM, respectively), in part caused by the decreased accuracy of the analysis at the lowest fluorophore concentration (Figure 20A). Nevertheless, binding of receptors **8** and **10** to peptide **1** was evidenced by a dose-dependent increase of fluorescence polarization in the absence of STAT1 (Figure 20B).

1.1.4 Conclusion

We have demonstrated the synthesis and use of artificial ditopic metal-chelate receptors for the binding of phosphorylated peptides and the inhibition of the interaction between human STAT1 and Chk2 proteins and their respective peptide binding sequences. The combination of a metal-chelate binding phosphorylated amino acids with a second binding moiety increasing the affinity and selectivity should be of general applicability, for example in the form of metal-chelate – peptide hybrid receptors.

1.1.5 Materials and Methods

Synthesis

Synthetic details and compound characterization data are provided in the supporting information of the publication of this chapter.²¹

Binding Studies to peptides **3** and **4**

All binding studies were conducted in buffered aqueous solution (50 mM HEPES buffer, pH 7.5, 154 mM NaCl) with an excitation wavelength of $\lambda_{\text{ex}} = 494$ nm at a constant temperature of 298 K. A Varian Cary Eclipse fluorometer was used for the emission titrations. The cuvette with peptide **3** or **4** in HEPES buffer was titrated stepwise with small amounts (beginning with 0.13 eq) of the receptor solution. After each addition the solution was allowed to equilibrate for 2 min before the fluorescence intensity and the UV spectrum (where permitted by the concentration range) were recorded. The stoichiometries were determined by Job's plots calculated from the titration data. To determine the binding constants, the obtained fluorescence intensities at 520 nm were volume corrected, plotted against the concentration of receptor and evaluated by nonlinear fitting.

Fluorescence-Titrations

Fluorescence titration results of the receptors **5** – **17** and the receptor substructures **18** and **19** against the test peptides **3** and **4** are shown below. The blue and red dots represent the measured data while the solid black lines represent the non linear fitting of the data.

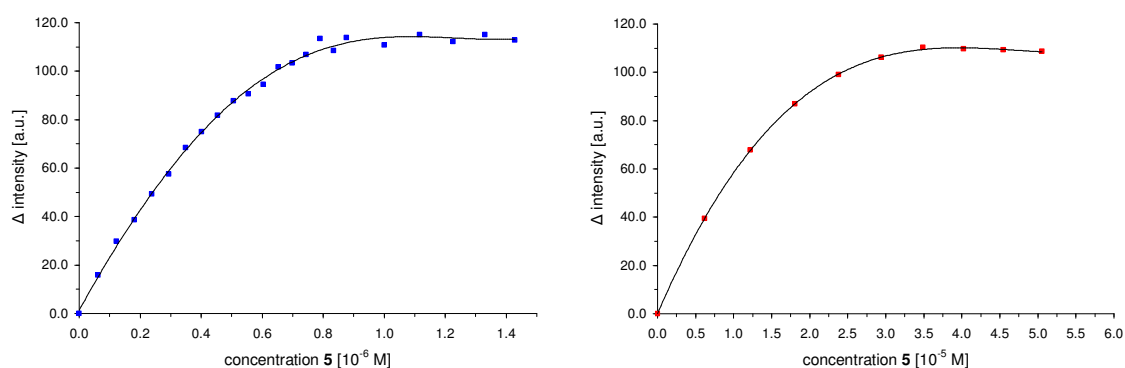


Figure 4. Emission titrations of receptor **5** against peptides **4** (left) and **3** (right).

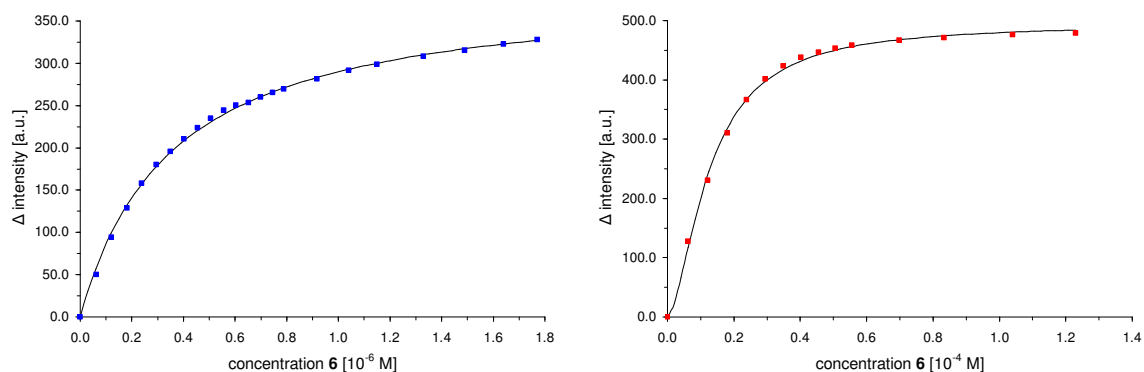


Figure 5. Emission titrations of receptor **6** against peptides **4** (left) and **3** (right).

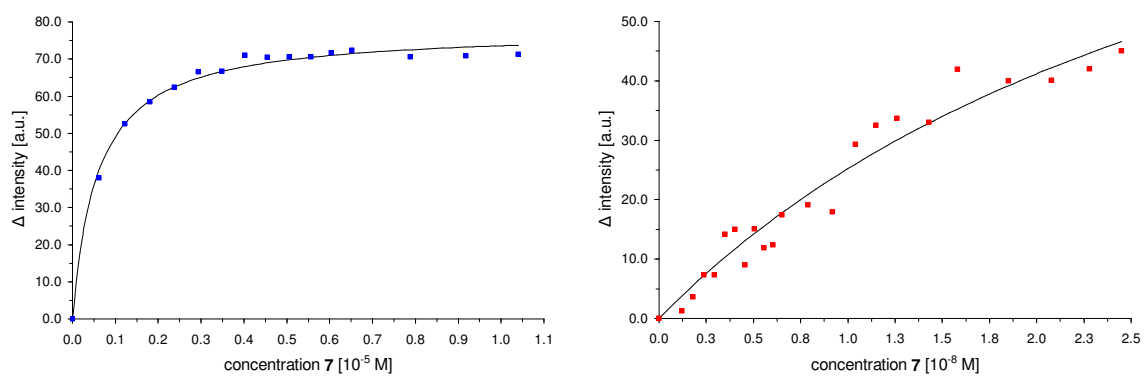


Figure 6. Emission titrations of receptor 7 against peptides 4 (left) and 3 (right).

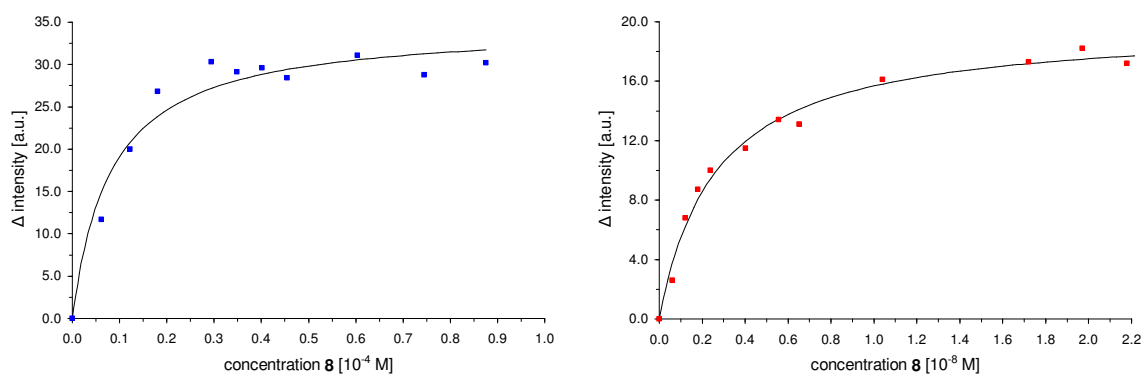


Figure 7. Emission titrations of receptor 8 against peptides 4 (left) and 3 (right).

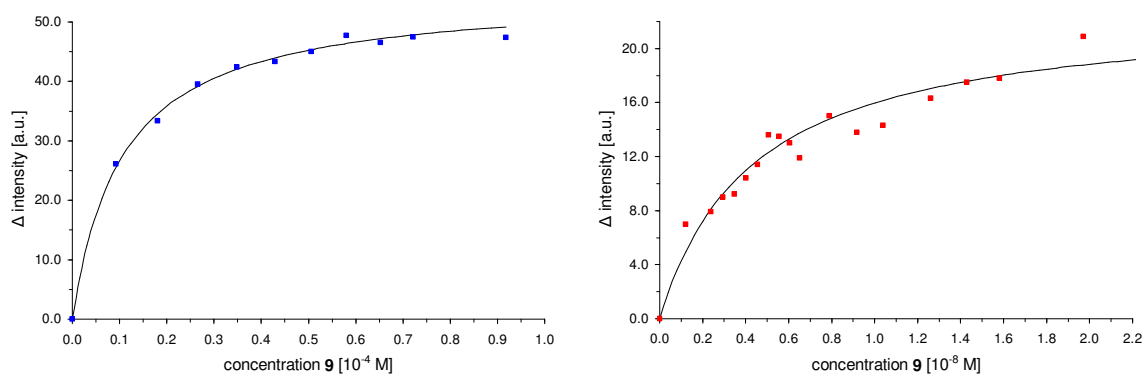


Figure 8. Emission titrations of receptor 9 against peptides 4 (left) and 3 (right).

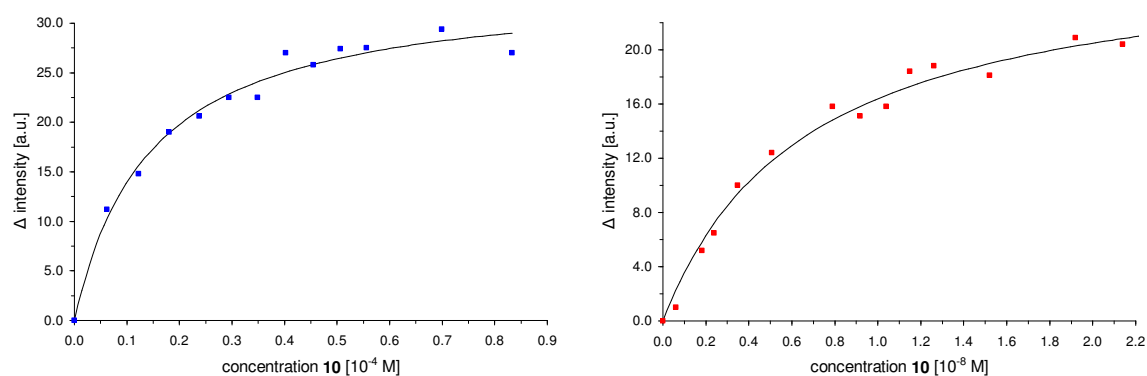


Figure 9. Emission titrations of receptor **10** against peptides **4** (left) and **3** (right).

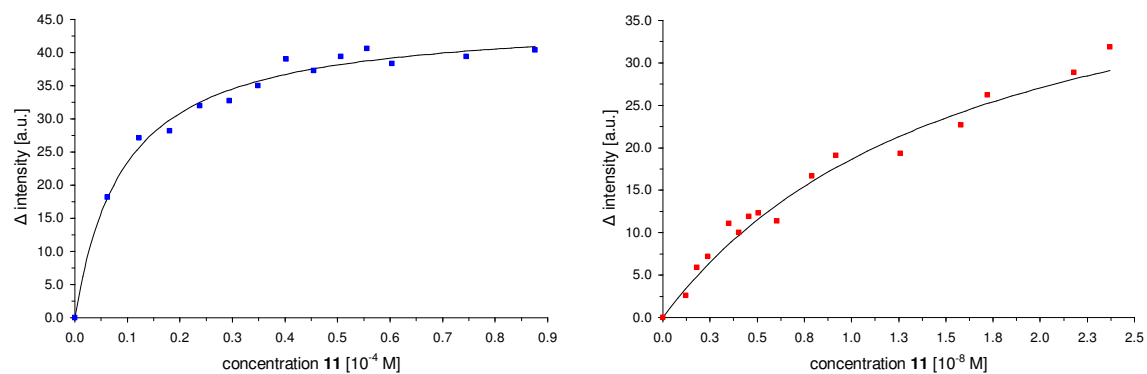


Figure 10. Emission titrations of receptor **11** against peptides **4** (left) and **3** (right).

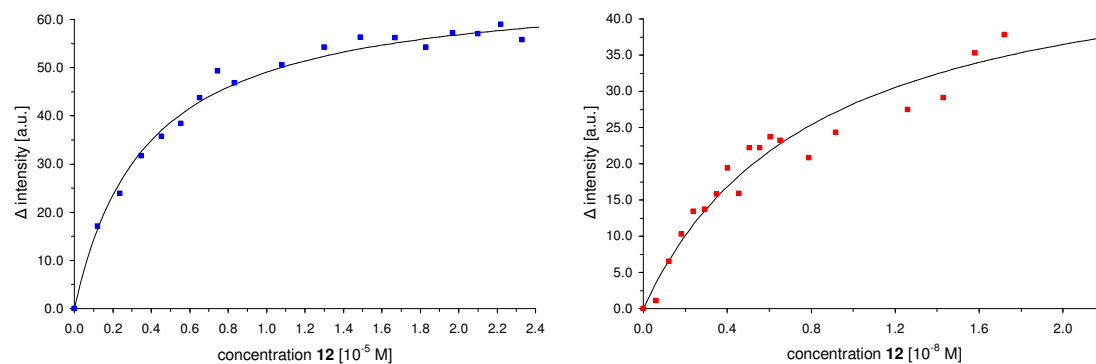


Figure 11. Emission titrations of receptor **12** against peptides **4** (left) and **3** (right).

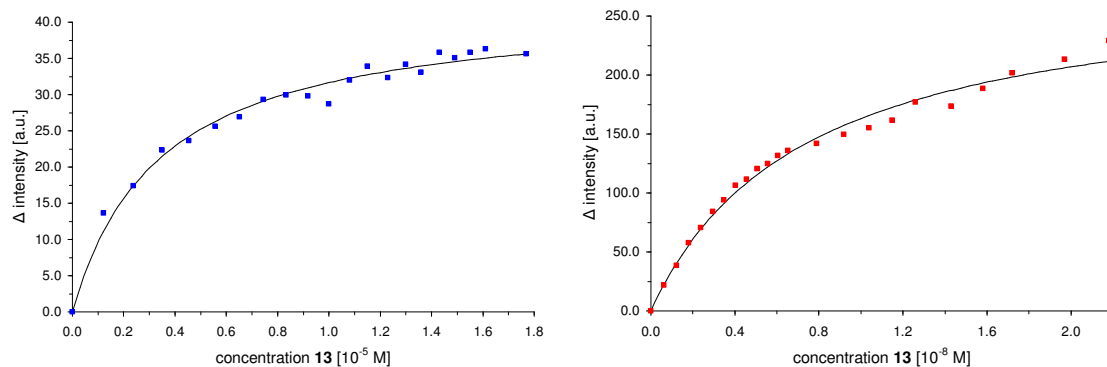


Figure 12. Emission titrations of receptor **13** against peptides **4** (left) and **3** (right).

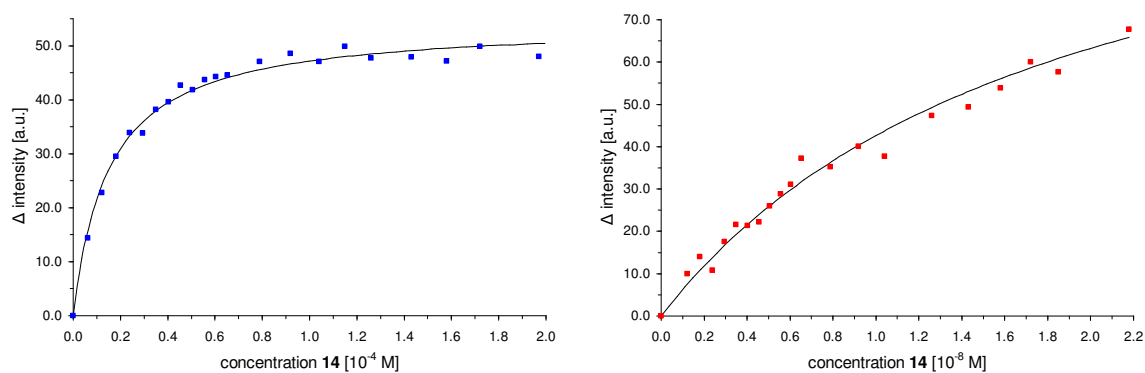


Figure 13. Emission titrations of receptor **14** against peptides **4** (left) and **3** (right).

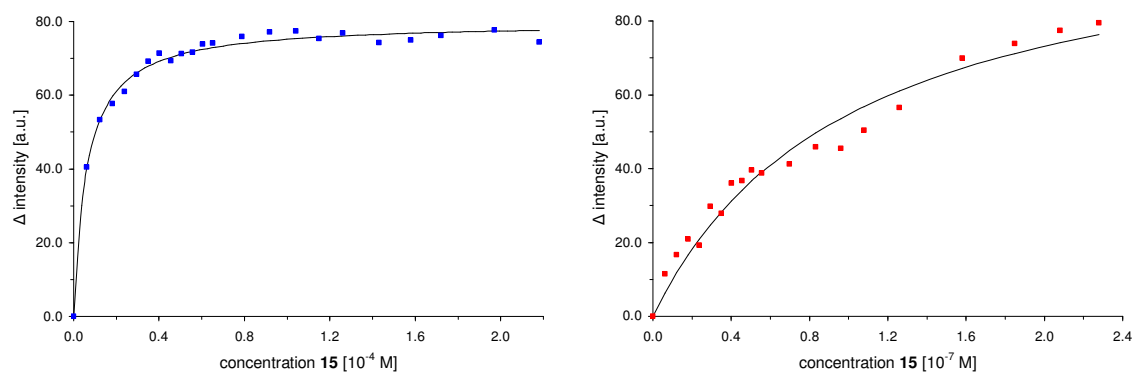


Figure 14. Emission titrations of receptor **15** against peptides **4** (left) and **3** (right).

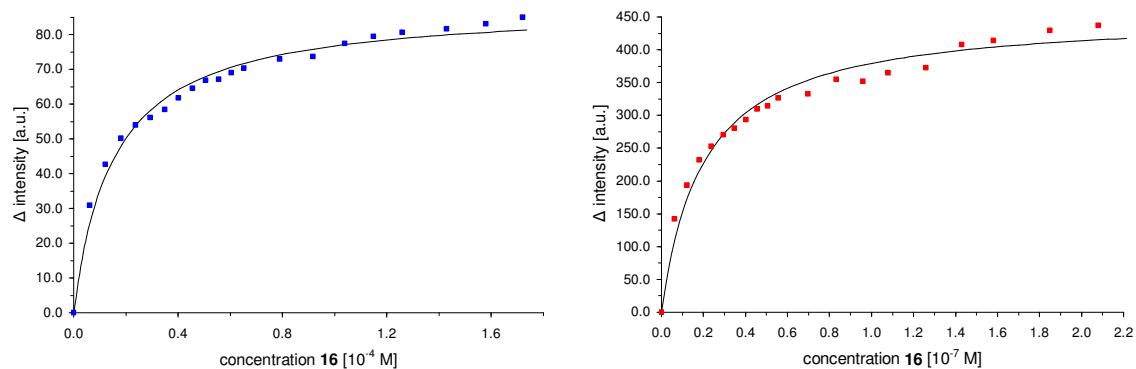


Figure 15. Emission titrations of receptor **16** against peptides **4** (left) and **3** (right).

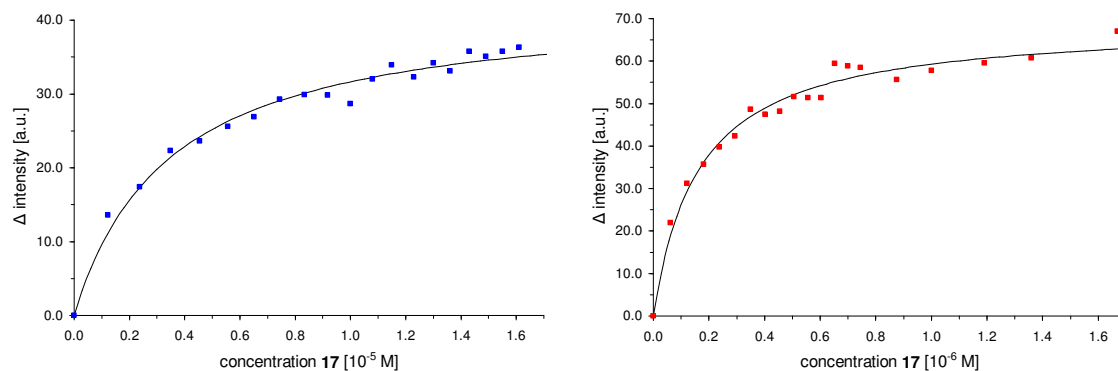


Figure 16. Emission titrations of receptor **17** against peptides **4** (left) and **3** (right).

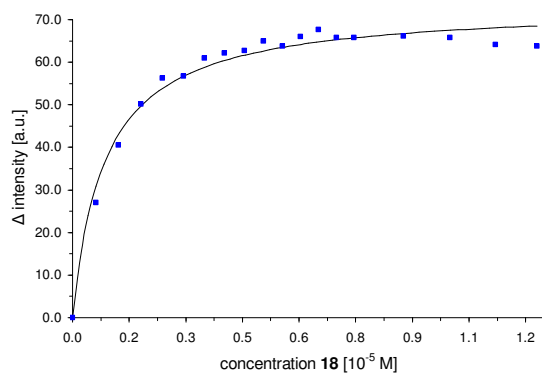


Figure 17. Emission titration of complex **18** representing a receptor substructure against peptide **4**.

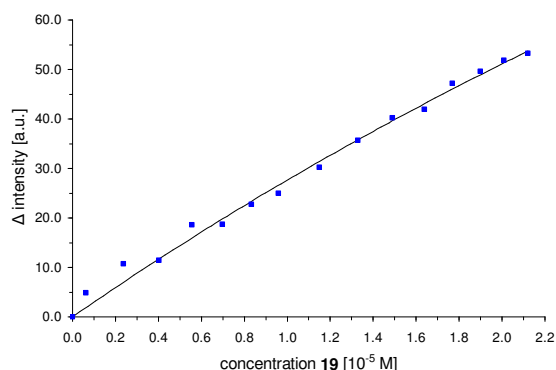


Figure 18. Emission titration of complex **19** representing a receptor substructure against peptide **4**.

Inhibition studies of peptide 1 – STAT1 and peptide 2 – Chk2 interactions

The test compounds were dissolved in 10 mM Tris pH 7.5. Expression and purification of STAT1 and the Chk2 FHA domain have been described.³ Binding assays were performed similarly as described.³ In brief, 30 μ L of a 16.7 nM solution of either 5-carboxyfluorescein-GpYDKPHVL (for STAT1) or 5-carboxyfluorescein-GHFDpTYLIRR (for Chk2) were incubated with a 5x stock solution of the test compounds (10 μ L) for 15 min at room temperature. Subsequently, 10 μ L of protein (STAT1: 400 nM; Chk2: 600 nM) was added and the mixture was allowed to equilibrate for 15 min. The solutions of the fluorescein-labeled peptides and the proteins were prepared in buffer containing 10 mM HEPES (pH 7.5), 1 mM EDTA, 0.1% Nonidet P-40, and 50 mM NaCl. Final concentrations: fluorescein-labeled peptides 10 nM; STAT1 80 nM; Chk2 120 nM. Fluorescence polarization was analyzed at room temperature in 384-well plates. All measurements were repeated three times in independent experiments.

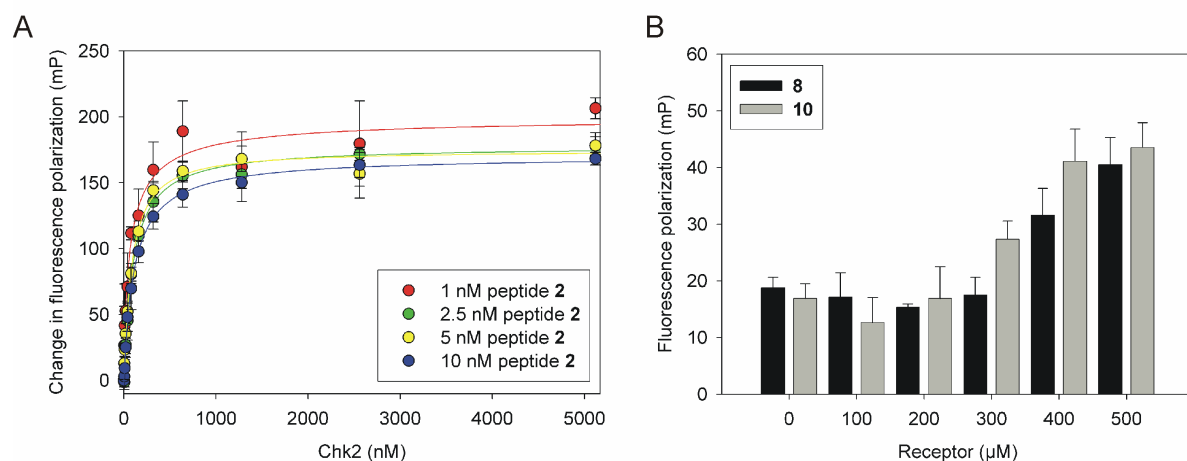


Figure 19. (A) Binding of peptide **2** to the Chk2 FHA domain analyzed by fluorescence polarization. The fluorescence polarization of peptide **2** in the absence of protein was subtracted from all experimental values. (B) Binding of receptors **8** and **10** to 10 nM of peptide **2** analyzed by fluorescence polarization.

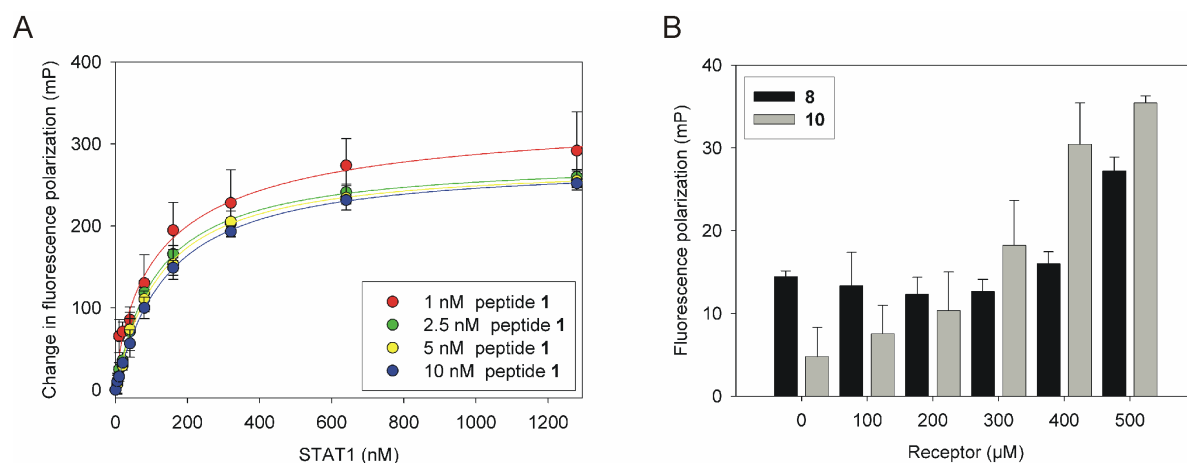


Figure 20. (A) Binding of peptide **1** to the STAT1 SH2 domain analyzed by fluorescence polarization. The fluorescence polarization of peptide **1** in the absence of protein was subtracted from all experimental values. (B) Binding of receptors **8** and **10** to 10 nM of peptide **1** analyzed by fluorescence polarization.

1.2 Detection of protein phosphorylation on SDS-PAGE

1.2.1 Introduction

Staining of SDS gels is a standard technique in molecular biology. While silver- and Coomassie-staining are widely used for total protein staining, a number of stains selective for certain functional groups have emerged. Glycosylation,^{22, 23} His-tags²⁴ and phosphorylation^{25, 26} are typical protein modifications targeted by selective gel stains reported so far. With respect to its biological importance, phosphorylation^{1, 2} is widely regarded as the most significant post-translational modification. Phosphorylation plays an important part in signaling pathways and it is estimated that 30 % of the entire proteome becomes phosphorylated at some point.²⁷ While there are phospho-specific antibodies available,^{28, 29} they require blotting of the proteins onto a polyvinylidene difluoride (PVDF) or nitrocellulose membrane and may also be specific for additional epitopes in proximity to the phosphorylation site. Alternatively, ³²P-labeling of the proteins provides a very sensitive tool for detection of phosphorylation,^{30, 31} however, the handling and disposal of radioactive material are costly, potentially hazardous and increasingly regulated. When staining for sub-stoichiometric features such as phosphorylation, fluorescence detection is the method of choice due to its inherent sensitivity. The reported³² and commercially available^{25, 26} fluorescent phospho-specific stains gain their sensitivity from their binding site specificity. While other fluorescent probes for phosphorylated amino acids have been reported,³³ their selectivity has only been demonstrated for peptides without other metal-chelating amino acids like histidine, tryptophan or cysteine.

Herein, we report two novel phospho-specific gel stains based on the interaction of a metal-chelate binding site and a covalently attached fluorophore. We have previously described the binding of a bis-zinc(II)-cyclen triazine to phosphorylated serine and histidine.¹² Since these artificial receptors showed high affinity under physiological conditions, we set about using this interaction in molecular biology. Based on these findings and a previously reported mono-zinc(II)-cyclen coumarin receptor³⁴ which changes its emission wavelength when bound to inorganic phosphate in solution, we designed fluorescently labeled bis-zinc(II)-cyclen triazine complexes for staining of phosphorylated proteins in SDS gels. Bis-zinc(II)-cyclen triazine was found to have a higher affinity towards phosphate than mononuclear

zinc(II)-cyclen complexes and was therefore used as the recognition moiety. As fluorophores, we selected the widely employed carboxyfluorescein and 7-(diethylamino) coumarin since a similar fluorophore has shown large solvatochromic emission shifts³⁵ which we associate to its sensitivity to the environment.³⁶ The resulting probes **1** and **2** are depicted in Figure 1 while the emission response concept is shown in Scheme 1.

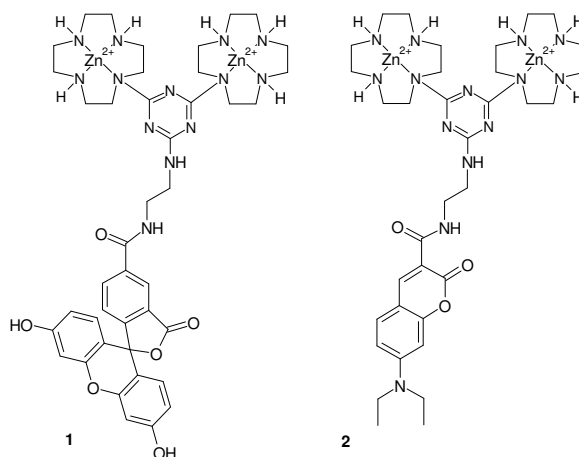
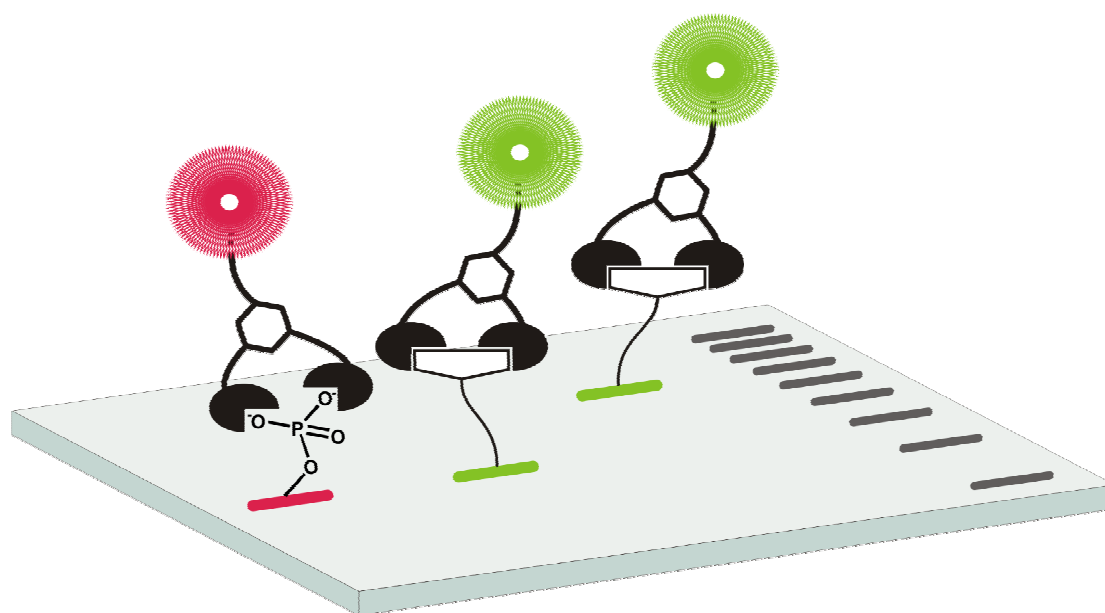


Figure 1. Probes **1** and **2** used for staining of phosphoproteins. Counterions are not shown.

1.2.2 Results and Discussion of the phosphostaining

To evaluate the phospho-staining selectivity and sensitivity of our probes, a dilution series of phosphorylated bovine α -casein was electrophoretically resolved from the non-phosphorylated protein BSA. In addition, a sample of α -casein was dephosphorylated using λ -PPase and used as a control to ensure the emission response would not depend on the amino acid composition of the protein. After fixation, the gels were stained and destained when necessary until little or no background was visible.



Scheme 1. Probes **1** and **2** discriminate phosphorylated from nonphosphorylated proteins on SDS gels via emission intensity and wavelength shift, respectively.

Probe **1** showed a distinct emission in the bands of phosphorylated α -casein, whereas the bands of dephosphorylated α -casein and BSA are barely visible (Figure 2). Bis-zinc(II)-cyclen triazine complexes coordinate phosphate groups strongly, but we also expect an affinity of the probe to non-phosphorylated proteins due to the coordination of histidine by the bis-zinc(II)-cyclen triazine^{12, 37} or further unspecific interactions. However, these interactions do not interfere with the specific detection of phosphorylation: The emission of the probe is quenched, when bound to non-phosphorylated amino acid residues and the emission remains, when bound to phosphorylated amino acid residues. Similar emission quenching effects have been previously reported for the interaction of riboflavin with a zinc(II)-imidazole complex³⁸ and for zinc(II)-porphyrin with histidine.³⁹ To prove that the observed effects originate from the coordination of the bis-zinc(II)-cyclen triazine complex and not from the binding of the fluorophore itself, a control gel was prepared and treated with carboxyfluorescein. No staining could be observed in this experiment.

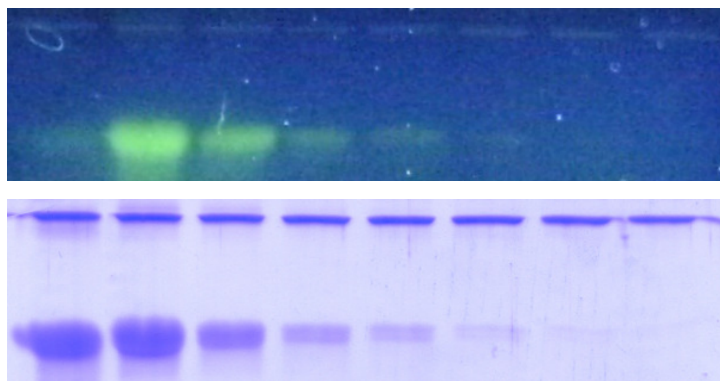


Figure 2. Gel stained with probe **1**. Each lane contains 1 μ g BSA (66 kDa). From left to right: lane 1: 1 μ g α -Casein (23 kDa) dephosphorylated, lanes 2 – 8: 1 μ g, 500 ng, 250 ng, 125 ng, 62 ng, 31 ng, 15 ng α -Casein. Top image was taken on a UV table ($\lambda_{\text{ex}} = 316$ nm), lower image shows CBB R-250 total protein restain.

When bound to phosphorylated α -casein, probe **2** showed a strong redshift in the emission compared to unphosphorylated α -casein and BSA (Figure 3). We attribute this spectral change to the different electronic environments when the probe molecule is either unspecifically interacting with non-phosphorylated amino acid residues, such as histidine (unphosphorylated α -casein and BSA) or is coordinating a negatively charged phosphorylated amino acid residue (phosphorylated α -casein). These findings are in agreement with the reported redshift in emission of a mono-zinc(II)-cyclen coumarin complex upon coordination to inorganic phosphate ions.³⁴ To quantify this change in emission, fluorescence spectra of the gel bands were obtained using a photonic multi-channel analyzer equipped with a fiber optic (Figure 4). As with probe **1**, a control gel was treated with the fluorophore itself, and again no staining was observed.

With both probes, the dilution series proved that 62 ng of phosphorylated α -casein are still detectable on a normal UV-table by the unaided eye (which was protected from UV light) while imaging was performed with common digital cameras. Hence, even without the use of specialized equipment like laser-illuminated gel scanners or cooled camera detectors as described in the protocols of commercially available phosphoprotein gel stains our probes reach similar limits of detection.

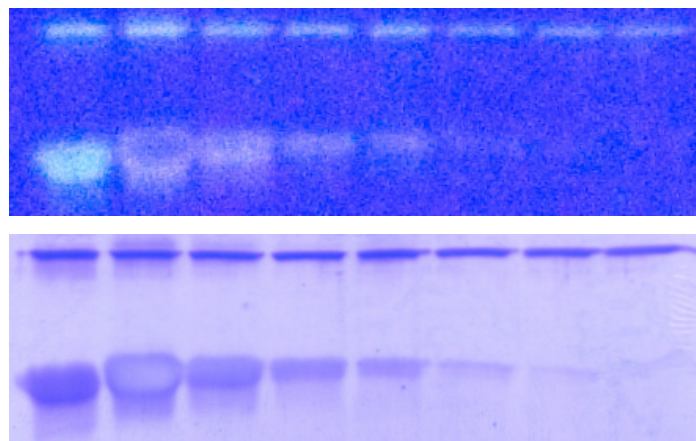


Figure 3. Gel stained with probe **2**. Each lane contains 1 μg BSA (66 kDa). From left to right: lane 1: 1 μg α -Casein (23 kDa) dephosphorylated, lanes 2 – 8: 1 μg , 500 ng, 250 ng, 125 ng, 62 ng, 31 ng, 15 ng α -Casein. Top image was taken on a UV table ($\lambda_{\text{ex}} = 316 \text{ nm}$), lower image shows CBB R-250 total protein restain.

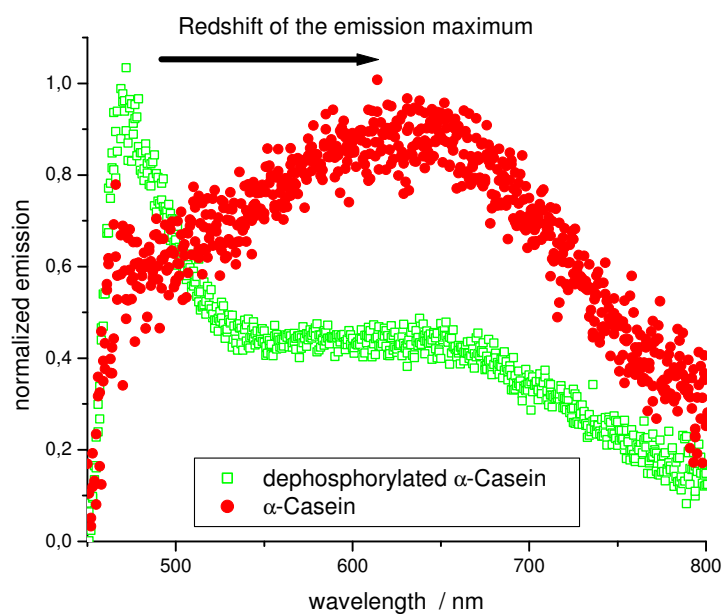


Figure 4. Normalized emission spectra of gel bands stained with probe **2** acquired through a 455 nm longpass filter ($\lambda_{\text{ex}} = 316 \text{ nm}$). BSA band showed the same spectrum as dephosphorylated α -casein (data not shown).

1.2.3 Conclusion

We have demonstrated the application of two new non-covalent, reversible and fluorescent SDS-PAGE probes capable of indicating protein phosphorylation. The probes show different fluorescence responses discriminating phosphorylated from non-phosphorylated proteins. While probe **1** signals binding to a phosphorylated protein by a significant increase of emission intensity, probe **2** is the first phosphoprotein gel stain to change its emission spectrum upon binding to a phosphorylated protein. The probes achieve their selectivity through a combination of the specificity of the dinuclear metal chelate binding site towards phosphate oxoanions and a modulation of the chromophore emission due to the proximity of the phosphorylated amino acid. The environment-sensitive fluorophores allow a clear distinction between phosphorylated and non-phosphorylated proteins on SDS-PAGE and allow the detection of 62 ng of phosphorylated α -casein on a normal UV-table. Evaluations of other metal chelate fluorophore conjugates and applications of the existing probes to monitor signaling pathways are currently under way.

1.2.4 Materials and Methods

Synthesis

Detailed information on the synthetic procedures and compound characterization data are provided in the supporting information of the publication of this chapter.⁴⁰

Dephosphorylation by λ -PPase treatment

Bovine α -casein (40 μ g, purchased from Sigma-Aldrich) was treated with 400 U of λ -PPase (purchased from New England Biolabs) in Tris-HCl (50 mM), NaCl (100 mM), dithiothreitol (2 mM), MnCl₂ (2 mM), EGTA (0.1 mM), 0.01 % Brij 35, pH 7.5 at 30 °C for 6 h.

SDS-PAGE

Proteins were resolved on mini gels under denaturing and reducing Laemmli conditions on a PeqLab 45-1010-i apparatus. The gels consisted of a 4 % acrylamide (w/v), 120 mM Tris-HCl (pH 6.8), 0.1 % SDS (w/v) stacking gel and a 15 % acrylamide (w/v), 375 mM Tris-HCl (pH 8.8), 0.1 % SDS (w/v) running gel. A 25 mM Tris, 192 mM glycine, 0.1 % SDS (w/v)

running buffer (pH 8.3) was used. Protein samples were heated to 70 °C for 10 min with reducing and denaturing RotiLoad 1 sample buffer (purchased from Carl Roth, Germany) before being loaded onto the gel. The gels were run at 150 V until the proteins entered the running gel, then the voltage was increased to 250 V. Water cooling was used during the entire run. Fixation was accomplished by treating the gels with 50 % MeOH, 10 % AcOH twice, for 30 min and overnight, respectively.

Staining and Imaging

The gels were soaked in deionized water (4 x 10 min) before being treated with a solution of probe **1** or **2** in deionized water for 1 h with a probe concentration of 10^{-7} M. We found destaining was not strictly necessary at this concentration, however, when the probes were used at higher concentrations, the gels could be destained by washing with deionized water until a nonfluorescent background was obtained. Due to their non-covalent binding mode,⁶ the probes could be completely removed by repeated washing of the gel with water. Conveniently, removal of the probes was not necessary for Coomassie restaining.

The gels were wrapped in cling film to prevent them from drying out and placed on a PeqLab Superbright UV table ($\lambda_{\text{ex}} = 316$ nm). Images were taken using either a Pentax K10D or a Traveler DC 8500. Emission spectra of individual protein bands were obtained using the same UV table and a Hamamatsu PMA-11 photonic multi-channel analyzer. Data were acquired using the supplied PMA Optic software. A 455 nm longpass filter was placed on top of the gel to prevent the UV light saturating the detector. Longpass filters with a shorter cutoff proved unsuitable as they showed a strong fluorescence when subjected to the UV light.

After fluorescence imaging, a restain for total protein was accomplished with 0.1 % Coomassie R-250, 50 % MeOH, 10 % AcOH for 1 h. Destaining was accomplished in 7 % AcOH, 10 % MeOH over night. The gels were again wrapped in cling film and scanned using an office scanner.

2. Inhibition of melanoma inhibitory activity (MIA) protein

The results presented in this chapter were achieved in collaboration with other scientists. I have focused on peptide synthesis, establishing the HTFP assay and screening the peptide libraries as well as performing other *in vitro* analyses such as Western blotting. J. Schmidt has performed most of the cell culture experiments, including all immunofluorescence studies and cloning. R. Stoll has conducted the NMR experiments, while C. Hellerbrand and T. Amann have helped conducting the animal experiments. W. Gronwald and F. Fink have performed the *in silico* studies. B. König and A. K. Bosserhoff have been supervising this project.

The results of this chapter have been either published or submitted for publication:

Riechers, A., Schmidt, J., König, B., Bosserhoff, A. K. Heterogeneous Transition Metal-based Fluorescence Polarization (HTFP) Assay for Probing Protein Interactions. *Biotechniques* **2009**, *47*, 837 – 844.

Schmidt, J., Riechers, A., Stoll, R., Amann, T., Fink, F., Hellerbrand, C., Gronwald, W., König, B., Bosserhoff, A. K. Dissociation of functionally active MIA protein dimers by dodecapeptide AR71 strongly reduces formation of metastases in malignant melanoma. *Nat. Med.* **2010**, (submitted).

2.1 Development of a screening assay for inhibitors of melanoma inhibitory activity (MIA) protein

2.1.1 Introduction

Protein interactions play a fundamental role in many biochemical processes like signal transduction, immune reaction, cell cycle control, differentiation and protein folding. The search for potent and selective inhibitors for specific protein-protein binding events is essential in pharmaceutical drug design and various techniques have been established for probing protein interactions. One commonly used screening method is an in-solution fluorescence polarization (FP) assay; in this technique, the rotational mobility of a fluorescently labeled entity is assessed in order to provide information about whether it is in a bound or unbound state. Clearly, this method is dependent upon a significant difference in molecular weight between the unbound fluorescently labeled entity versus when it is part of a binding complex. Here, we describe a high-throughput FP-based screening assay that is compatible with both high and low molecular weight interaction partners.

We have termed our method the heterogeneous transition metal-based fluorescence polarization (HTFP) assay. Compared to organic fluorophores, luminescent transition metal complexes have a number of advantages, such as a large Stokes shift, high photostability and the option to be used in time-gated measurements. These time-gated measurements offer the possibility of multiple labeling using transition metals with different lifetimes despite possible spectral overlap and the elimination of autofluorescence of biological material. Although luminescent transition metal complexes have been used in FP immunoassays,^{41, 42, 43, 44, 45, 46, 47, 48, 49, 50, 51, 52, 53} these reagents are not feasible for use in binding investigations of low molecular weight compounds in solution, for example in drug candidate screening, due to the dependence of fluorescence polarization on molecular weight and fluorescence lifetime. Therefore, instead of performing the assay in free solution, we have anchored one of the binding factors to the surface of a well in a multiwell plate. This surface-bound factor is then incubated with its fluorescently labeled protein partner and other compounds being tested for binding activity. In the absence of a competitive inhibitor, the protein is tethered to the well's surface and has limited ability to rotate. However, in the presence of a compound that can compete away the binding between the protein and its immobilized binding partner, the

protein is freed into solution, and the resulting increase in its rotational diffusion can be easily detected by FP measurements.

We demonstrate the HTFP assay in a screen of melanoma inhibitory activity (MIA) protein inhibitors. MIA protein, an 11 kDa molecule produced under physiological conditions by cartilage, is strongly expressed and secreted by malignant melanoma cells, but is not expressed in melanocytes.^{54, 55} Since MIA protein expression level *in vivo* directly correlates with progressive malignancy of melanocytic tumors, it serves as a reliable clinical tumor marker to detect and monitor metastatic diseases.^{56, 57} Recent data describe a direct interaction of MIA protein with the cell adhesion receptors integrin $\alpha_4\beta_1$ and integrin $\alpha_5\beta_1$ and with extracellular matrix molecules, including fibronectin.^{58, 59} By modulating integrin activity and masking matrix structures, MIA protein mediates detachment of melanoma cells, resulting in enhanced invasive and migratory potential that ultimately contributes significantly to the formation of metastasis.⁶⁰ To prevent metastasis, it is desirable to find substances that specifically bind to MIA protein and thereby reduce MIA-induced effects. Here, MIA and known binding partners were used to develop the HTFP assay as a high-throughput method to identify and characterize protein interactions.

2.1.2 Results of the HTFP assay studies

In previous studies, FN14, a peptide that matches a fibronectin domain, was identified as an MIA binder in a phage display experiment.⁶¹ AR54, an MIA-binding peptide deduced from peptide FN14, has been shown by Boyden Chamber invasion assay to functionally inhibit MIA protein *in vitro*. The peptide was able to almost completely inhibit MIA protein function by preventing interactions of MIA protein with extracellular matrix molecules and integrins without affecting cell migration itself.⁶² Using AR54 as a known inhibitor of MIA protein, we aimed to establish an assay which allows detection of potential MIA-inhibitory compounds.

Commonly used methods for investigating protein interactions, like fluorescence emission titration (a method that is generally used to obtain information about stoichiometry and binding constants) and fluorescence resonance energy transfer (FRET)-based experiments, were found to be inappropriate. This failure was due to inherent tendency of MIA protein to form aggregates;⁶¹ moreover, a FRET experiment with an N-methylantraniloyl labelled AR54 derivative failed due to spectral overlap. Since dynamic light scattering (DLS), nuclear magnetic resonance (NMR), and isothermal titration calorimetry (ITC) were not sensitive

enough to detect binding events at physiologically relevant concentrations, we decided to employ FP for elucidating the interaction of MIA protein with AR54.

FP experiments with a carboxyfluorescein-labeled derivative were compromised by nonspecific interactions of both MIA protein and the respective control protein with the fluorophore. We therefore reevaluated the choice of our assay format and decided to establish a new FP-based assay in which the protein rather than the inhibitor was labeled. In this scenario, we envisioned that the change in molecular weight resulting from binding would be observable only if the labeled protein of interest (MIA) was bound by an inhibitory compound (AR54) immobilized to a well plate (Figure 1). The FP signal should decrease after competitive displacement of labeled MIA protein from immobilized AR54 by an inhibitory compound.

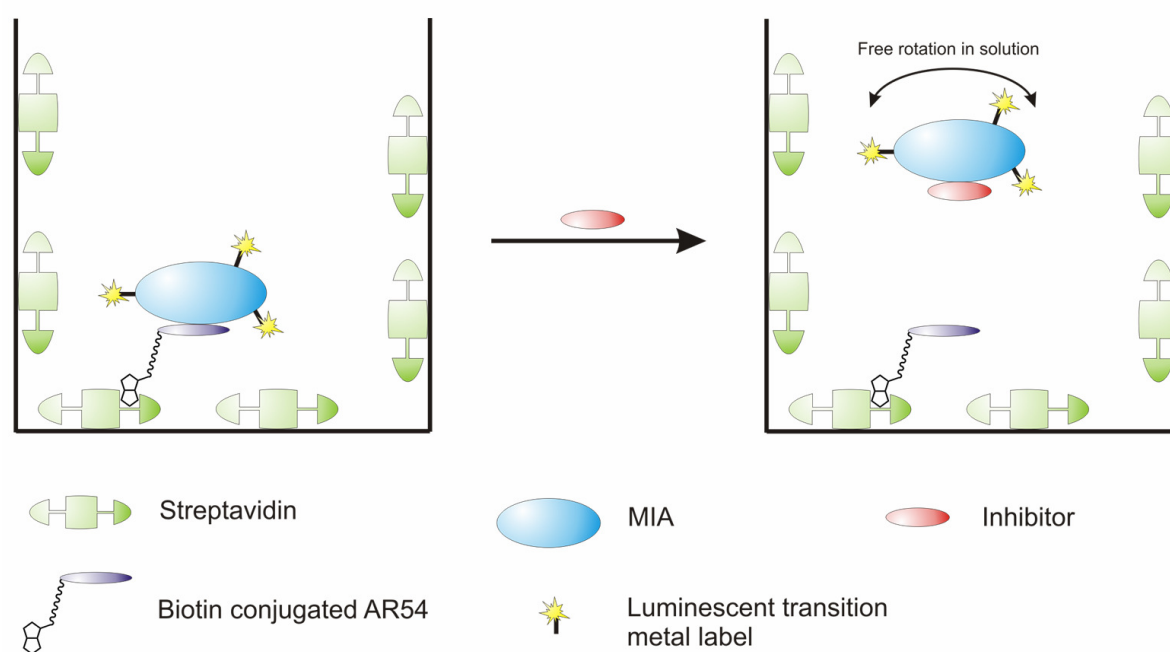


Figure 1. Concept of the FP assay using a luminescent transition metal complex as the label. Binding of Ru(bpy)₃-labeled MIA protein to the immobilized inhibitory peptide AR54 leads to a large change in molecular weight, resulting in a dramatic increase of the fluorescence polarization signal (left). After competitive displacement of labeled MIA protein from immobilized AR54 by an inhibitory compound (right) the FP signal decreases. The HTPFP assay should enable high-throughput screening of large substance libraries for potent MIA protein inhibitors.

As a label, we chose the luminescent Ru(bpy)₃ (tris(2,2'-bipyridine)ruthenium (II)) complex due to its sufficiently long lifetime. To ensure that Ru(bpy)₃ does not affect binding properties of MIA protein, we performed Boyden Chamber invasion experiments, where Mel Im cells were treated with Ru(bpy)₃-labeled MIA protein and, in comparison, with unlabeled MIA protein. Non-modified MIA protein reduces cell invasion by about 40 % to 50 % in this *in vitro* model because MIA protein specifically interferes with attachment of melanoma cells to matrigel.⁶⁰ We found that unlabeled and labeled MIA protein behave identically, confirming that Ru(bpy)₃-labeled MIA is functionally active (data not shown).

Binding of MIA-Ru(bpy)₃ to AR54, 30 kDa and 70 kDa fibronectin fragments

First, we measured the FP signal of MIA-Ru(bpy)₃ in a well coated with AR54-biotin compared to an uncoated well. The significant increase in FP in the well coated with AR54-biotin was attributed to the severely restricted rotational mobility of MIA-Ru(bpy)₃ bound to the immobilized AR54-biotin (Figure 2). In order to assess whether we could displace MIA-Ru(bpy)₃ from the immobilized AR54-biotin, we treated this complex with 7.8 μM AR54 in solution. In this case, the FP of MIA-Ru(bpy)₃ was almost identical to MIA-Ru(bpy)₃ free in solution (in a well not coated with AR54-biotin). This demonstrates that the molecular mobility is unhindered and that the binding is reversible.

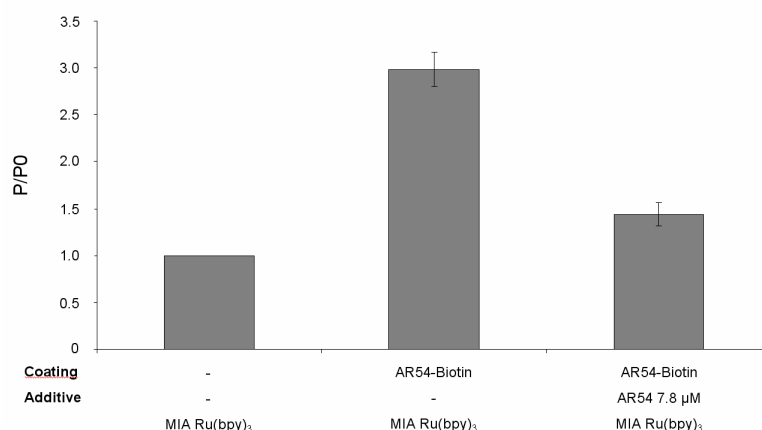


Figure 2. HTFP assay investigation of interaction of AR54 with MIA-Ru(bpy)₃. In the AR54-biotin treated well, the FP signal increases due to binding of Ru(bpy)₃-labeled MIA protein to immobilized AR54 peptide. After addition of AR54 at a final concentration of 7.8 μM, the detected FP of MIA-Ru(bpy)₃ is almost identical to the MIA-Ru(bpy)₃ free in solution (in a well not coated with AR54-biotin), demonstrating that after displacement from immobilized AR54-biotin, the molecular mobility is unhindered.

The interaction of MIA with fibronectin has been described previously.⁵⁹ In order to test our assay with this known interaction partner, we applied 30 kDa and 70 kDa proteolytic fragments of human fibronectin, as shown in Figure 3A. As expected, FP decreased upon addition of the fibronectin fragments. Taken together with the AR54 results, this finding demonstrates that our HTFP assay is capable of detecting protein interactions with a small peptide as well as a 70 kDa protein.

Next, we performed a titration of MIA-Ru(bpy)₃ with the 30 kDa fibronectin fragment to demonstrate that our assay is also capable of determining binding constants. As presented in Figure 3B, we determined a K_d value of 33 nM.

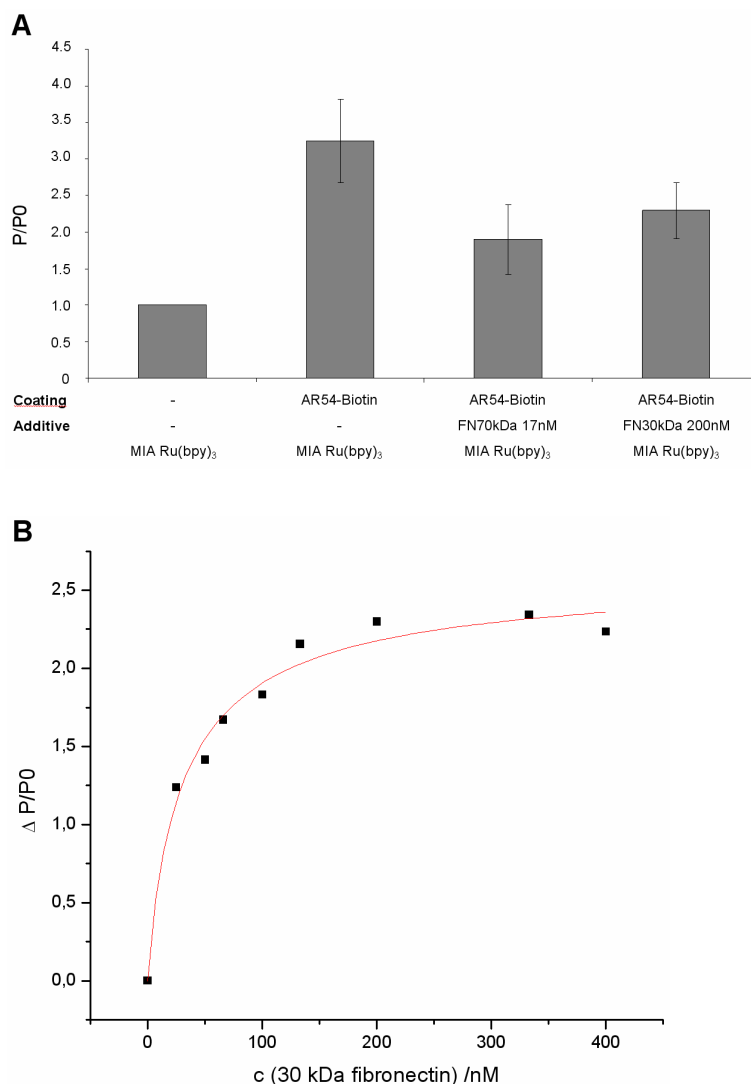


Figure 3. HTFP assay investigation of interaction of 30 kDa and 70 kDa fibronectin fragments with MIA-Ru-(bpy)₃. (A) 30 kDa and 70 kDa proteolytic fragments of human fibronectin, known to interact with MIA protein, were applied in the HTFP assay. The FP

signal decreases, indicating a displacement of MIA protein from AR54-Biotin. **(B)** Titration of MIA-Ru(bpy)₃ with 30 kDa human proteolytic fibronectin fragment. The observed K_d is 33 nM. All experiments were performed in triplicate.

Buffer additives and detergent controls

To assess the suitability of the HTFP assay as a screening platform for the identification of potential MIA protein inhibitors, we investigated the influence of various buffer additives and detergents commonly used in molecular biology. As expected, the addition of 0.1 % Triton X-100 or 0.1 % 2-mercaptoethanol disrupted the interaction of MIA-Ru(bpy)₃ and AR54-biotin (data not shown). DMSO, which is often used in inhibitor screenings for dissolving compound libraries, could be tolerated for concentrations of up to 2.5 %, but the addition of 50 mM EDTA (ethylenediamine tetraacetic acid) induced a significant decrease in FP signal (data not shown). This can be explained by a photoinduced redox reaction involving the luminescent label Ru(bpy)₃ and EDTA.⁶³ Consistent with this proposed mechanism, a similar decrease was also observed in the absence of AR54-biotin.

Multimerization studies

Although aggregation can lead to artifacts in other binding experiments, we hypothesized that our assay, with its long lifetime of the luminescent label, should be beneficial for investigating proteins prone to multimerization. The addition of an excess of unlabeled MIA protein to MIA-Ru(bpy)₃ does not change FP (Figure 4A), indicating that the size of the multimers does not change and that there are no aggregates consisting of about ten or more molecules. We estimate this from the lifetime of the label and the molecular weight of the protein by the Perrin equation. To demonstrate the existence of smaller aggregates, we coated wells with a MIA-biotin conjugate. Indeed, a large increase in FP was detected, indicating the presence of direct MIA-MIA interactions. The formation of multimeric structures of MIA protein was also confirmed by Western blot analysis as shown in Figure 4B. These aggregates appear to be extraordinarily stable since they can even be observed after treatment with denaturing and reducing Laemmli buffer at 70 °C.

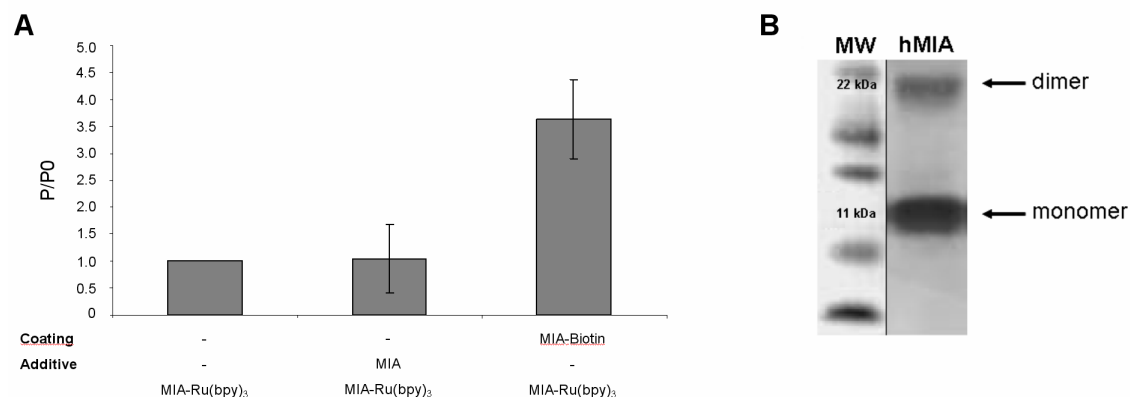


Figure 4. HTFP assay investigation of MIA protein aggregation. **(A)** Analysis of MIA aggregation was performed under physiological conditions using DPBS buffer in an AR54-uncoated well. **(B)** As also demonstrated by Western blot analysis, 11 kDa MIA protein forms multimeric structures. All experiments were performed in triplicate.

2.1.3 Discussion of the HTFP assay studies

Several methods have been developed for the investigation of protein interactions. While surface plasmon resonance (SPR) ⁶⁴ can also be used for small-molecule interactions with the help of antibodies, it is still costly because proprietary chips are generally required. Far-Western blotting is time consuming and also not suitable for high-throughput applications.⁶⁵ Furthermore, this method relies on the refolding of the protein to its native conformation on the membrane, which may not always be successful. Immunoprecipitation and pull-down experiments are also far more time-consuming than fluorescence-based investigations.⁶⁶ Binding experiments using the 1-anilino-8-naphthalene sulfonate (ANS) probe,⁶⁷ while compatible with multiwell plate-based assays, suffer from short excitation and emission wavelengths. Automated isothermal calorimetry measurements offer the advantage of label-free detection, but still require relatively large amounts of substance.

Methods capable of handling high-throughput screening include various types of microarrays using enzymes, isotopes, or fluorescent labels. However, these techniques require special safety precautions, antibodies, and washing steps that may lead to cross-contamination and other artifacts.

FP detection is both high-throughput capable and self-referenced, meaning that no washing steps are required. This is clearly an advantage over the traditional ELISA (enzyme-linked

immunosorbent assay) platform. Traditional homogeneous FP assays are limited by the molecular weight of the interaction partner to be investigated, due to the short lifetime of the required organic fluorophores. We extend this range by immobilizing a known interaction partner of the protein of interest, which is itself labeled with a long-lifetime luminescent transition metal chelate. The maximum acceptable molecular weight of the interaction partner obviously depends on the decay time of the label on the target. Given the decay time of Ru(bpy)₃, we estimate from the Perrin equation⁶⁸ that interactions with binding partners of up to 500 kDa should still be observable, however, that limit could be raised by using a transition metal with a longer decay time.

The results show that our HTFP assay allows the investigation of protein-small molecule as well as protein-protein interactions. Thus, in contrast to traditional homogeneous FP assays, interactions with both high and low molecular weight compounds can be investigated. As presented for the interaction of MIA protein with AR54, this FP assay should also be amenable for the screening of libraries of potential drug candidates. Additionally, our HTFP assay is suitable for the investigation of protein aggregation and compounds cleaving these aggregates. This tolerance of the HTFP assay for aggregation makes it unique and should allow the investigation of proteins which show aggregation-related artifacts in other assays. However, one limitation of our assay is the fact that it will be difficult to estimate aggregate sizes from the polarization values due to the long decay time.

Since our assay format is applicable to a variety of situations, it is conceivable that it also might be used for other analytical or diagnostic applications. For instance, the HTFP assay would be expected to enable the investigation of protein complexes, such as cell signaling molecules, transport proteins, or transcription factors. It could also be used for the identification of an initiator or regulator of polymerization reactions, for instance for actin or tubulin subunits within the dynamic processes of the cytoskeleton. This assay may also serve to identify activators or co-activators for enzymatic reactions as well as for the design of immunoassays in the field of serology and diagnostics. Since the HTFP assay is based on a luminescent transition metal complex label, it benefits from all the associated advantages over organic fluorophores. While the inherent photostability is obviously convenient, the large Stokes shift increases the signal-to-noise ratio and allows a broader selection of suitable emission filters for the spectrometer. Furthermore, the long lifetime of transition metal complex labels also opens the possibility of time-gated measurements. This may be employed for multi-label experiments with different transition metal complexes of different lifetimes, allowing these labels to be resolved regardless of spectral overlap. Finally, complex biological

matrices in the samples are also tolerable because the autofluorescence of biological material has a very short lifetime and can thus be eliminated.

2.1.4 Materials and Methods

Cell lines and cell culture conditions

The melanoma cell line Mel Im, established from a human metastatic tumor sample (a generous gift from Dr. Johnson, University of Munich, Germany), was used in Boyden Chamber invasion experiments. Cells were maintained in DMEM (Dulbecco's Modified Eagle Medium; PAA Laboratories GmbH, Austria) supplemented with penicillin (400 U/mL), streptomycin (50 µg/mL), l-glutamine (300 µg/mL) and 10 % fetal calf serum (Pan Biotech GmbH, Germany) and split in a 1:5 ratio every three days.

Boyden Chamber Invasion Assay

Invasion assays were performed in Boyden Chambers containing polycarbonate filters with 8 µm pore size (Neuro Probe, Gaithersburg, MD, USA) essentially as described previously.⁶⁹ Filters were coated with Matrigel, a commercially available reconstituted basement membrane (diluted 1:3 in H₂O; BD Bioscience, Bradford, MA, USA). The lower compartment was filled with fibroblast-conditioned medium used as a chemoattractant. Mel Im melanoma cells were harvested by trypsinization for 2 min, resuspended in DMEM without fetal calf serum (FCS) at a density 2.5×10^4 cells/mL, and placed in the upper compartment of the chamber. Except for the control experiment with untreated cells and experiments where cells were only treated with the peptide, MIA protein or Ru(bpy)₃-labeled MIA protein, respectively, was added to the cell suspension at a final concentration of 200 ng/mL. Peptide AR54 (sequence: NSLLVSFQPPRAR) was used at a final concentration of 1 µM. After incubation at 37° C for 4 h filters were removed. Cells adhering to the lower surface of the filter were fixed, stained, and counted. Experiments were carried out in triplicates and repeated at least three times.

Protein analysis by Western blotting

MIA protein was denaturated at 70°C for 10 min after addition of reducing and denaturing Roti-Load buffer (Roth, Karlsruhe, Germany) and subsequently separated on sodium dodecyl sulfate 12.75 % polyacrylamide gels (SDS-PAGE) (Invitrogen, Groningen, The Netherlands).

After transferring the proteins onto a polyvinylidene fluoride (PVDF) membrane (BioRad, Richmond, VA, USA), the membrane was blocked using 3 % bovine serum albumin (BSA) in phosphate-buffered saline (PBS) for 1 h at room temperature (RT) and incubated with a 1:150 dilution of primary polyclonal rabbit anti-MIA antibody (Biogenes, Berlin, Germany) in 3 % BSA/PBS overnight at 4°C. After washing in PBS the membrane was incubated with a 1:2000 dilution of an alkaline-phosphatase coupled secondary antibody (Chemikon, Hofheim, Germany) for 2 h at RT. Finally, after washing steps, immunoreactions were visualized by nitro blue tetrazolium/5-bromo-4-chloro-3-indolyl phosphate (NBT/BCIP) (Invitrogen) staining.

Luminescent labeling of human MIA protein

Human MIA protein (100 µg) was labeled with Ru(bpy)₃-isothiocyanate (1 mg) (Active Motif Chromeon, Germany, cat# 15412) in 640 µL bicarbonate buffer pH 9.3 supplemented with 200 µL DMSO (dimethylsulfoxide) required for dissolving the dye. After 50 min, the reaction mixture was purified on a size-exclusion column (SephadexTM G-25 M PD-10 Desalting column, Amersham Pharmacia Biotech, Sweden) and samples of the collected fractions as well as a dilution series of unlabeled MIA protein were analyzed by Western blotting as described above.

Biotin conjugation of peptide AR54

0.25 mg of AR54 was dissolved in 30 µL of bicarbonate buffer pH 9.3. After addition of 0.38 mg biotin-NHS ester (Calbiochem, USA, cat# 203188) in 10 µL DMSO the reaction mixture was incubated overnight at 4 °C. As the NHS-ester was expected to be completely reacted or hydrolyzed, no purification was carried out.

Coating of well plates with AR54-biotin and MIA-biotin

Black streptavidin-coated 96 well plates (Greiner Bio-one, Germany, cat# 655997) with a loading of 20 pmol streptavidin per well were treated with 20 equivalents AR54-biotin per mol of (tetrameric) streptavidin in PBS pH 7.4. An uncoated control lane was sealed with adhesive film to prevent contamination with AR54-biotin. After addition of AR54-biotin, the entire plate was sealed with adhesive film and incubated for 3 h under agitation. The coated lanes were washed five times with PBS pH 7.4 before being air-dried and sealed with adhesive film which was removed only immediately before use of each lane.

MIA-biotin was prepared as previously reported⁵⁹ and used for treating a well plate as described above, except that the plate was not dried and used for measurements immediately.

Polarization assay setup

All measurements were performed at room temperature on a Polarstar Optima microplate reader (BMG Labtech, Germany). A 390-10 nm bandpass filter was used for excitation while a 520 nm longpass filter was used for the emission light. Even though the extinction coefficient is higher at longer wavelengths, we chose a shorter excitation wavelength as this led to higher polarization values. A MIA-Ru(bpy)₃ concentration of 55 fM was used in all experiments. A solution volume of 250 µL per well was found to give a low standard deviation with high signal intensity. Unless otherwise indicated, all measurements were performed in DPBS without calcium or magnesium (PAN Biotech GmbH, Germany). Addition of components to the wells was done in the following order: Interaction partner, buffer, MIA-Ru(bpy)₃. Owing to different reaction kinetics, measurements were performed every 5 min over a 30 min period. Polarization values are reported relative (P/P_0) to the value of free MIA-Ru(bpy)₃ in solution in a well not treated with AR54-Biotin. All reported values are an average of three independent measurements.

2.2 Dissociation of functionally active MIA dimers by dodecapeptide AR71 strongly reduces formation of metastases in malignant melanoma

2.2.1 Introduction

Malignant melanoma is characterized by aggressive local growth and early formation of metastases. In order to identify autocrine growth-regulatory factors secreted by melanoma cells, melanoma inhibitory activity (MIA), an 11 kDa protein, strongly expressed and secreted by melanocytic tumor cells was purified from tissue culture supernatant of the human melanoma cell line HTZ-19.^{54, 70} Today it serves as a reliable clinical serum tumor marker for detection of metastatic diseases and monitoring therapy responses of patients suffering from malignant melanoma. In addition, MIA plays an important functional role in melanoma development and cell invasion as its expression levels directly correlate with the capability of melanoma cells to form metastases in syngeneic animals.^{60, 71, 72}

After transcription, MIA mRNA is translated into a 131 amino acid precursor molecule and processed into a mature protein consisting of 107 amino acids after cleavage of the secretion signal sequence.⁷⁰ The transport of MIA protein to the cell rear is induced after migratory stimuli.⁷³ Following secretion, MIA subsequently binds to cell adhesion receptors integrin $\alpha_4\beta_1$ and integrin $\alpha_5\beta_1$. In addition, MIA masks their binding sites at ECM molecules including fibronectin, laminin and tenascin.^{59, 60} Consequently, cell adhesion contacts are reduced, enabling tumor cells to migrate and invade into healthy tissue, resulting in enhanced metastatic potential.

Previously, the three-dimensional structure of MIA protein was solved by multidimensional nuclear magnetic resonance (NMR) spectroscopy and X-ray crystallography techniques.^{74, 75, 61, 76, 77} Corresponding data indicated that MIA defines a novel type of secreted protein comprising an SH3 domain like fold.

In the present study we aimed to determine the so far unknown molecular mechanism of MIA. By functionally analyzing MIA mutants we demonstrate for the first time that MIA achieves functional activity by self assembly. Peptidic dimerization inhibitors were identified and analyzed in *in vitro* and *in vivo* studies, thus providing an excellent starting point for the development of a new inhibitory strategy. Based on these new data presented here, the rational design and development of a novel pharmacophore which inhibits MIA and thus

strongly reduces tumor cell invasion and formation of metastases could provide a key element in malignant melanoma therapy.

2.2.2 Results of the inhibition studies

MIA protein is functionally active as a dimer

Although MIA was thought to act as a monomer, recent data suggests that, as detailed below, the active form of the protein consists of a dimer. Using the PreBI modelling software (<http://pre-s.protein.osaka-u.ac.jp/prebi/>) for the prediction of the putative dimer interface together with the HADDOCK protein-protein docking program,⁷⁸ we obtained a model of the MIA dimer comprising a head to tail linkage (Figure 1A). The dimerization interfaces are located around Y30 and at the region K53-L58 in the n-Src loop and the cleft next to Q65-A73 in the distal loop. Further supporting our results, the regions determined to form the interface have been described as crucial for functional activity in a previous mutagenesis study.⁶⁹ In addition, Western blot analysis of MIA also demonstrates that apart from the monomeric species dimers exist.⁷⁹ We, therefore, aimed to investigate the physiological relevance of MIA dimers and the possible correlation between dimerization and functional activity. Having identified the most likely positions of the dimerization interfaces, mutants of MIA were tested for their capability to form dimers by Western blot analysis (Figure 1B). MIA mutants were expressed in an *in vitro* transcription/translation system. All mutants showed correct folding as evidenced by an MIA-ELISA and were selected as not carrying a mutation in the dimerization regions, apart from G61R.⁶⁹ Recombinant wt MIA and all mutants clearly show a dimer band except for G61R. Interestingly, all mutants but G61R are functionally active in Boyden chamber invasion assays, as presented in Figure 1C. MIA wt (RTS) and mutants D29G/Y69H, V46F/S81P, T89P and K91N can exhibit this effect to the same extent while MIA mutant G61R completely loses activity. The sites of mutations not affecting functional activity (Figure 1D, depicted in grey) are located outside the dimerization regions, whereas G61R (Figure 1D, depicted in magenta) is buried in the dimerization cleft (depicted in red) in close proximity to the distal loop.

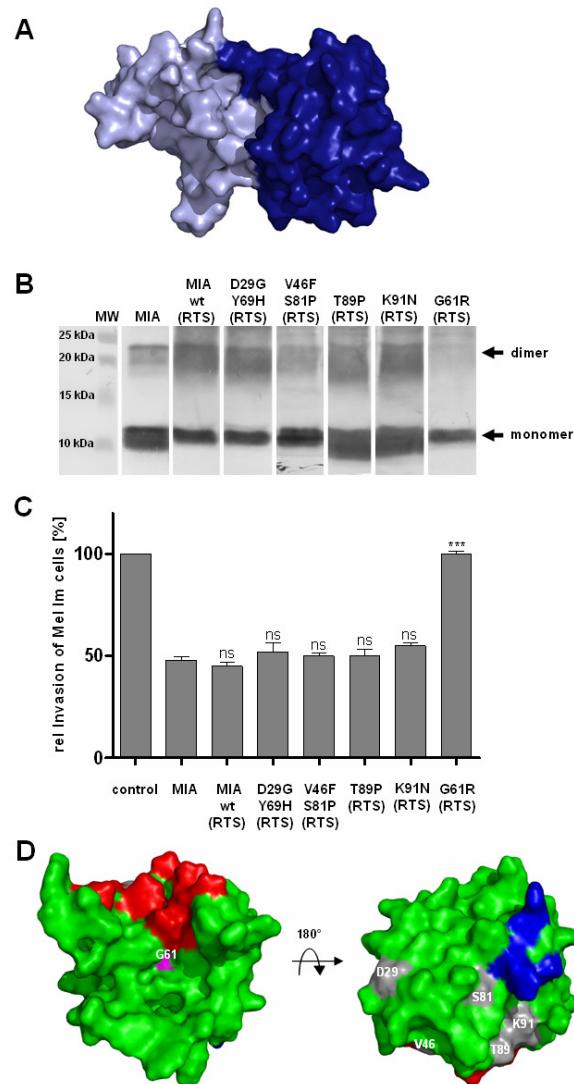


Figure 1. MIA protein is functionally inactive as a monomer. **(A)** Structure of the MIA dimer according to shape complementarity analyses. The MIA dimer is characterized by a head-to-tail orientation, with the dimerization domains consisting of the n-Src loop and the cleft next to the distal loop. **(B)** Western blot analysis of MIA mutants assessing their ability to form dimers. The first lane shows recombinant wt MIA, followed by the same protein in an unpurified RTS expression system (wt) and mutants D29G/Y69H, V46F/S81P, T89P, K91N and G61R. All homologues, except for G61R, clearly show a dimer band. **(C)** Correlation between dimerization and functional activity revealed that all MIA mutants capable to dimerize are functionally active in Boyden chamber invasion assays as reflected by a reduction in the number of invaded cells due to interference with cell adhesion. Mutant G61R, which does not form protein dimers does not show any MIA induced effect. **(D)** NMR structure of MIA showing the dimerization domains and the mutation sites. The dimerization

domains in the n-Src loop and next to the distal loop are depicted in blue and red, respectively. Mutation sites which do not influence dimerization and functional activity are shown in grey and obviously lie outside the dimerization domains. The site of mutation G61R, which is in direct contact with the dimerization domain next to the distal loop, is shown in magenta. This figure was generated using PyMol (Delano, W. L., The PyMol Molecular Graphics System (2002) Delano Scientific, Palo Alto, CA, USA).

Peptide AR71 prevents MIA protein dimerization

We then aimed to identify peptides inhibiting MIA dimerization in a newly developed heterogeneous transition-metal based fluorescence polarization (HTFP) assay.⁷⁹ First, MIA-MIA interaction was confirmed using this assay. Here, we immobilized a MIA-biotin conjugate in a streptavidin-coated well plate and added MIA labelled with the luminescent transition-metal complex Ru(bpy)₃. As depicted in Figure 2A, a significant increase in FP signal in the wells coated with MIA-biotin was observed compared to control wells not functionalized with MIA-biotin. This was attributed to the severely restricted rotational mobility of MIA-Ru(bpy)₃ bound to the immobilized MIA-biotin.

We then screened peptides, previously identified by phage display and known to generally bind to MIA,⁶¹ for their potential to prevent MIA dimerization and induce dissociation of already existing protein dimers using the HTFP assay. As shown in Figure 2A, peptide AR71 (sequence: Ac-FHWRYPLPLPGQ-NH₂) was found to be particularly potent in dissociating MIA dimers which led to a decrease in FP signal due to increased rotational diffusion of the dissociated monomeric MIA-Ru(bpy)₃. This effect of AR71 was confirmed by Western Blot analysis (Figure 2B). Preincubation of MIA with 1 µM peptide AR71 leads to a strong reduction of the dimer bands compared to the control lane or other MIA-binding peptides used (AR68, AR69).

To prove that AR71 functionally inhibits MIA, Boyden chamber invasion assays were performed (Figure 2C). In these *in vitro* experiments, MIA interferes with the attachment of cells to matrigel, as reflected by a decrease in cell invasion. After external treatment with MIA, invasion of Mel Im cells is significantly reduced about 40% to 50% compared to untreated control cells. Pre-incubation of MIA with the inhibitory peptide AR71 results in a complete neutralization of the effect caused by MIA, as reflected in the number of invaded cells. Treatment of cells with peptide AR71 alone does not influence the migratory behaviour of melanoma cells.

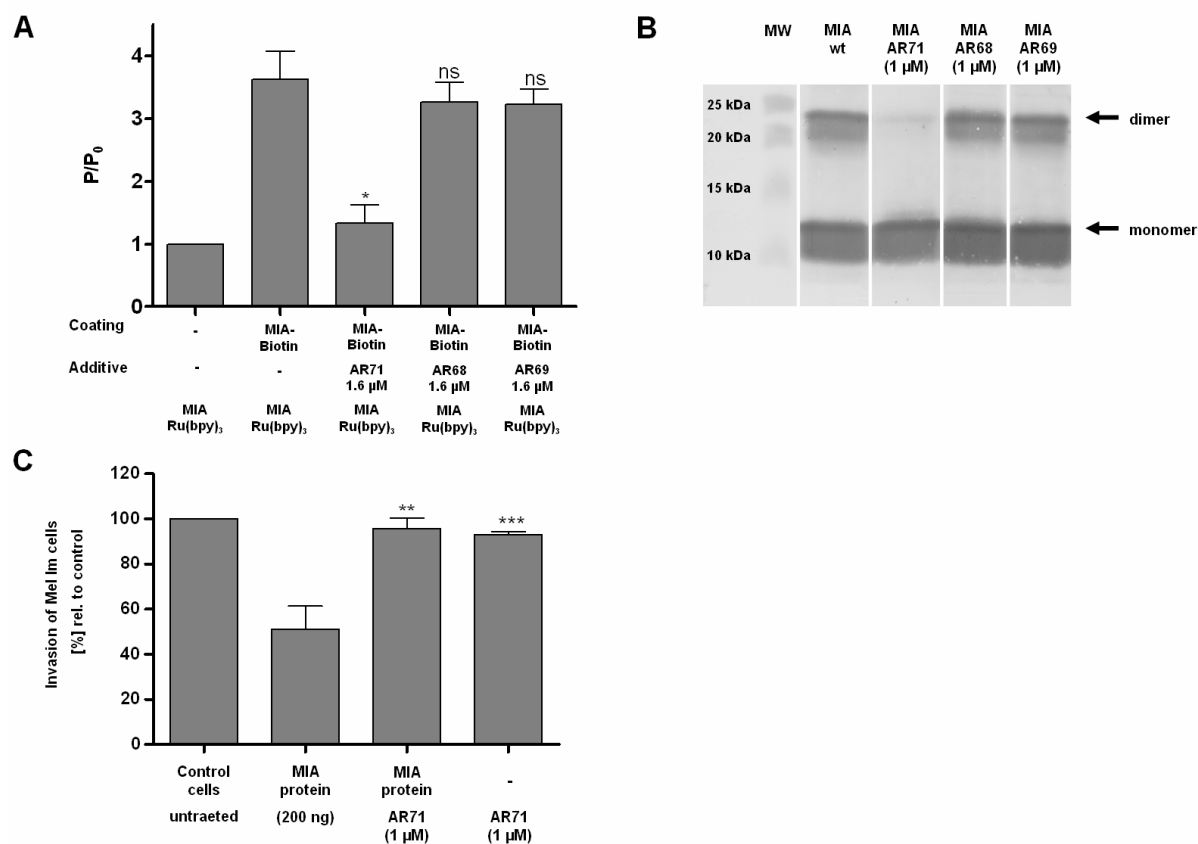


Figure 2. Peptide AR71 prevents MIA dimerization. **(A)** Heterogeneous transition-metal based fluorescence polarization (HTFP) assay for probing AR71 for its ability to directly interfere with MIA-MIA interaction. In the control lanes the FP signal of MIA- Ru(bpy)_3 was measured in a well coated with MIA-biotin compared to an uncoated well. The significant increase in FP in the well coated with MIA-biotin indicates binding of MIA- Ru(bpy)_3 to the immobilized MIA-biotin. The binding of MIA-inhibitory compound AR71 promotes dissociation of MIA dimers and displaces the surface-bound MIA- Ru(bpy)_3 , as reflected by the decrease in fluorescence polarization. Peptides AR68 and AR69, also derived from a phage display, do not interfere with MIA-MIA interaction. **(B)** Western Blot analysis of MIA incubated with 1 μM AR71 demonstrates peptide-induced dissociation of the dimer, as deduced by a strong reduction of the dimer band compared to the control lane. MIA-binding peptides AR68 and AR69 do not lead to reduced dimer formation. **(C)** Boyden chamber invasion assays using the human melanoma cell line Mel Im indicate that AR71 almost completely inhibits MIA activity. Interference of MIA with cell attachment to matrigel results in a decrease in cell invasion; after external treatment with MIA invasion of Mel Im cells is

significantly reduced about 40% to 50% compared to untreated control cells. Pre-incubation of MIA with the respective inhibitory peptide results in a complete neutralization of the MIA effect. The two control lanes confirm that AR71 alone does not influence the migratory behaviour since exposure of cells to the peptide in absence of MIA does not alter the quantity of migrated cells.

MIA interacts with AR71

After demonstrating the potential of AR71 to inhibit MIA function in *in vitro* models, we could show by multidimensional NMR spectroscopy that MIA binds to this peptide ligand. In addition, the potential binding site of AR71 was identified using ^{15}N labeled MIA and unlabeled peptide. By using increasing amounts of AR71 peptide, the induced chemical shift changes of the MIA $^1\text{H}^{\text{N}}$ and $^{15}\text{N}^{\text{H}}$ resonances were classified according to the degree of the combined chemical shift perturbations. Further analysis of the solvent accessibility (with a threshold of 20 %) and cluster analysis of the residues effected by peptide binding reveals that the binding interface potentially comprises residues C17, S18, Y47, G66, D67, L76, W102, D103 and C106 of MIA (Figure 3A) It can therefore be assumed that the peptide predominantly binds to the binding site depicted on the left side of Figure 3A, whereas the opposite side of the molecule most probably does not participate in binding.

After stably transfecting B16 mouse melanoma cells with a secretion-signal containing AR71-HisTag construct (Sig-AR71-HisTag), we first analysed expression and localization of endogenous AR71-HisTag peptide. Co-staining of MIA protein and AR71-HisTag revealed a colocalization in close proximity to the nucleus. Immunofluorescence studies show the localization of MIA (green, Figure 3Ba) and AR71-HisTag (for demonstrating colocalization with MIA, the red TRITC emission has been changed to yellow in this false-color illustration, Figure 3Bb). The colocalization, depicted in red, is indicated by white arrows in Figure 3Bc. The excess of MIA not colocalized with AR71 is due to internalization of exogenous MIA protein by the melanoma cells.⁶² Figure 3Bd shows the corresponding mock control.

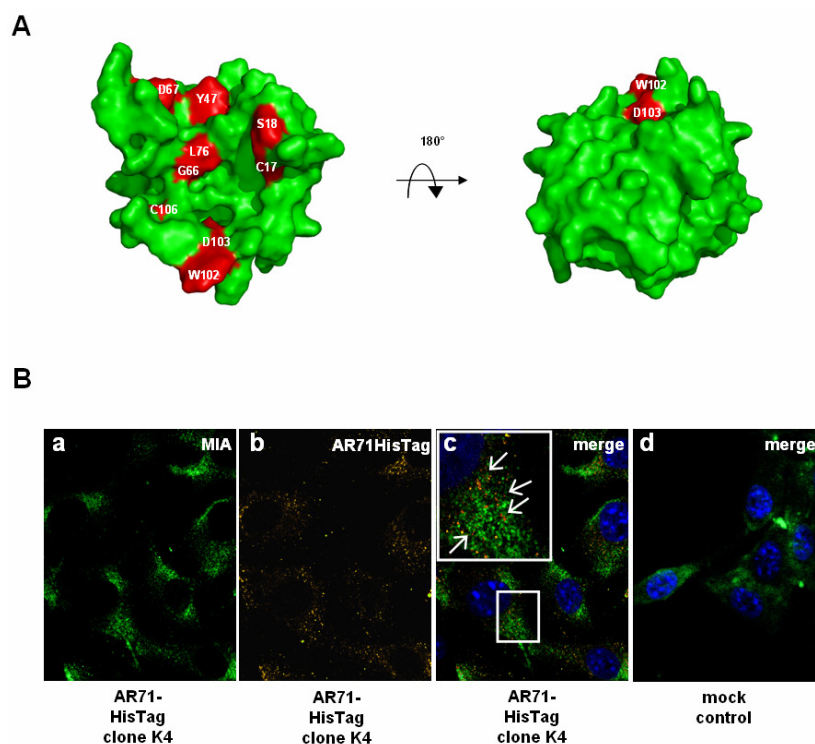


Figure 3. Chemical shift differences of MIA upon titration with the dodecapeptide AR71. **(A)** Most significant chemical shift differences projected onto the van der Waals surface of MIA upon titration with the peptide AR71 are shown in red. The binding site is located in the dimerization domain next to the distal loop (compare Figure 1D). This figure was generated using PyMol (Delano, W. L., The PyMol Molecular Graphics System (2002) Delano Scientific, Palo Alto, CA, USA). **(B)** Immunofluorescence studies of murine B16 melanoma cells stably transfected with a (Sig)-AR71-HisTag construct. While a) shows MIA (FITC) and b) displays AR71-HisTag (TRITC with color changed from red to yellow for better visualization of colocalization), colocalization shown in red is indicated by white arrows in c). d) Corresponding mock control without AR71-HisTag.

Effect of MIA inhibitory peptide AR71 on formation of metastases *in vivo*

MIA expression levels of malignant melanoma cells strictly correlate with a highly invasive phenotype *in vitro* and *in vivo*.^{57, 80, 81} Further, *in vivo* studies have demonstrated the strong contribution of MIA for melanoma cell invasion and migration.^{71, 72}

In order to assess the ability of peptide AR71 to inhibit the formation of metastases by generating inactive MIA monomers *in vivo*, a previously developed metastasis assay was employed.⁸² In this assay, melanoma cells metastasize from the primary tumor in the spleen via the portal vein into the liver. Nine days after injection of the cells into the spleen, the mice

were sacrificed, the livers were resected and tissue sections were prepared. Here, we used the stably transfected murine B16 melanoma cells with a Sig-AR71-HisTag containing construct. *In vitro* analysis by Boyden chamber assay confirmed that migration is drastically reduced in Sig-AR71-HisTag expressing cell clones compared to mock control cells (Figure 4A). The interference of AR71-HisTag with MIA-MIA interaction was also confirmed in the HTFP assay using wells coated with MIA-biotin (data not shown). Subsequently, a Sig-AR71-HisTag clone as well as a corresponding mock control was injected into the spleen of C57Bl6 mice, respectively. Histological analysis of haematoxylin and eosin stained liver sections revealed that mice being injected with Sig-AR71-HisTag clones comprised significantly fewer metastases than the mock control (Figure 4B). Four representative histological liver sections (hematoxylin and eosin stained) of mice injected with the B16 mock control or mice injected with the Sig-AR71-HisTag expressing cell clone, respectively, are shown in Figure 4C. Black arrows indicate the small metastases in the mock control which are exceedingly reduced in the liver of mice injected with the Sig-AR71-HisTag expressing cell clone. No adverse effects of AR71 on other organs and tissues were observed.

These results prompted us to investigate whether AR71 peptide could also reduce the formation of metastases when given as an *i.v.* administration treatment. Therefore, wild type murine B16 melanoma cells were injected into the spleen of C57Bl6 mice with the mice being subsequently treated with *i.v.* injections of AR71 (50 µg every 24 h). After nine days, the mice were sacrificed, the livers were resected and again tissue sections were prepared. Histological analyses revealed a significant reduction of the average number of metastases in the liver of mice treated with AR71 compared to the liver of untreated control mice, as shown in figure Figure 4D. Four representative histological liver sections (hematoxylin and eosin stained) of untreated and treated mice, respectively, are shown in Figure 4E. Again no adverse effects on other organs and tissues were observed.

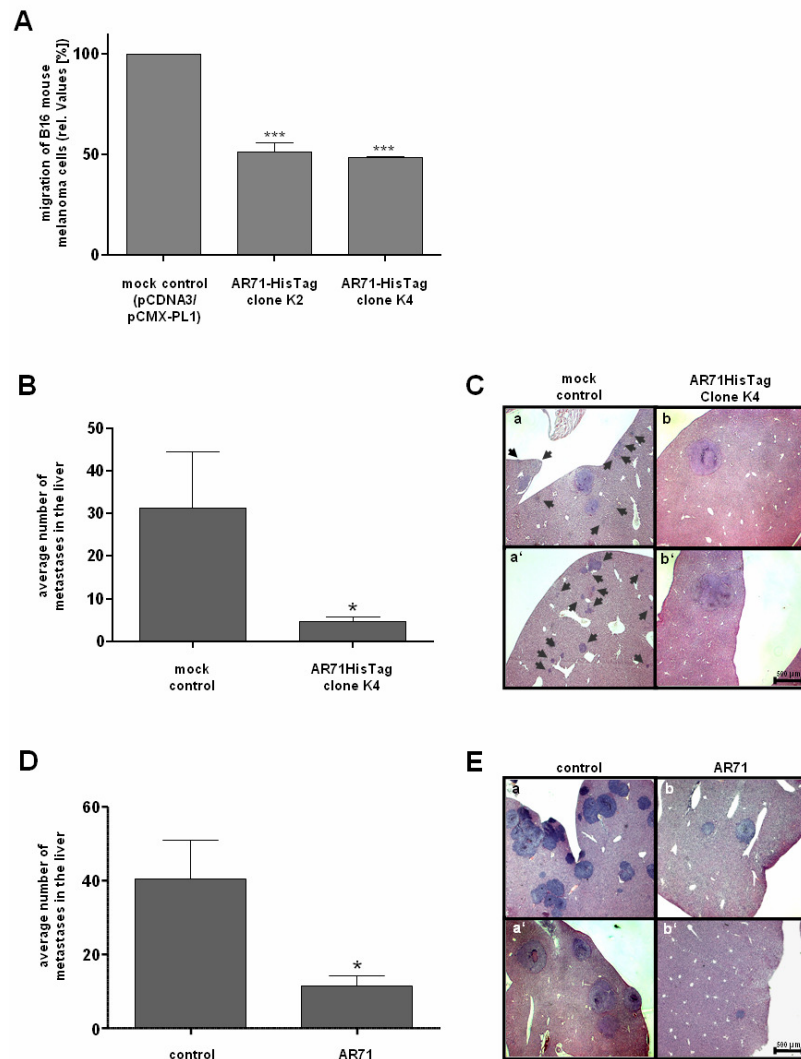


Figure 4. Effect of MIA inhibitory peptide AR71 on formation of metastases *in vivo*. **(A)** Murine B16 melanoma cells stably transfected with a (secretion-signal)-AR71-HisTag containing construct were analyzed for their migratory activity in a Boyden chamber assay. Compared to the mock control, migration is drastically reduced in the two Sig-AR71-HisTag expressing cell clones clone K2 and clone K4. **(B)** Sig-AR71-HisTag clone K4 as well as a corresponding mock control were injected into the spleen of B1/6N mice, respectively. Histological analysis of haematoxylin and eosin stained liver sections revealed that mice being injected with Sig-AR71-HisTag clones comprised significantly fewer metastases than the mock control. **(C)** Representative histological liver sections (hematoxylin and eosin stained), two of mice injected with the B16 mock control (a and a') and two of mice injected with the Sig-AR71-HisTag expressing cell clone K4 (b and b'). Black arrows indicate small metastases. **(D)** Wild type murine B16 melanoma cells were injected into the spleen of B1/6N

mice with the mice being subsequently treated with *i.v.* injections of AR71 (50 µg every 24 h). Histological analyses revealed a significant reduction of the average number of metastases in the liver of mice treated with AR71 compared to the liver of untreated control mice. **(E)** Representative histological liver sections (hematoxylin and eosin stained), two of untreated (a and a') and two of treated mice (b and b').

2.2.3 Discussion of the inhibition studies

Primary melanomas often reach a high proliferation rate and acquire competence for metastasis in early stages of the disease. As already presented in previous studies, MIA plays a fundamental role in this process.^{60, 71} However, hitherto the molecular mechanism by which MIA enables tumor cell release from the primary tumor and promotes formation of metastases elsewhere in the body was poorly understood.

Here, we newly describe that MIA is active as a dimer. MIA dimerization is supported by *in silico* studies as well as Western blot analysis, mutagenesis studies and HTFP assay measurements.⁷⁹ We identified the probable dimerization domains as being located in the n-Src loop and in the cleft next to the distal loop. Additionally, this tendency of MIA to form homomeric linkages was also indicated by previous NMR spectroscopy experiments revealing a transversal relaxation time (T_2) shorter than expected for an 11 kDa protein.^{76, 83}

However, until now, dimerization of MIA has not been correlated with functional activity. Our studies revealed that MIA is functionally inactive as a monomeric species and only wt MIA and MIA mutants still forming dimers were found to be functionally active in Boyden chamber invasion assays. The mutants D29G/Y69H, V46F/S81P, T89P and K91N are still able to dimerize. Replacement of these amino acids outside the dimerization domains in the n-Src loop and next to the distal loop does not hinder dimerization and consequently does not influence functional activity. In contrast, the mutation G61R is located at the dimerization interface next to the distal loop of MIA. In this mutant, glycine, an uncharged amino acid residue with minimum sterical demand is replaced by arginine, a positively charged and very large residue. As expected, this exchange strongly impacts formation of MIA dimers due to sterical demand and charge repulsion between the two respective MIA-MIA binding sites. The fact that monomeric MIA is functionally completely inactive suggests that the active site for integrin and ECM binding could potentially be generated by self assembly of two identical MIA subunits.

The concept of proteins that require dimerization in order to reach functional activity has been described for example for lipoprotein lipase which is converted into inactive monomers by angiopoietin-like protein 4. Concomitant with dissociation of functionally active dimers into monomers, an irreversible loss of catalytic activity was found.⁸⁴ Furthermore, this functional coupling between oligomerization and activity of proteins has also been reported for herpesvirus protease, which is also inactivated after dimer disruption.^{85, 86}

The feasibility of inhibiting protein activity via preventing dimerization was discussed in a study by Wlodawer *et al.* describing a similar mechanism for inhibiting HIV-1 protease, a homodimeric protein requiring dimerization for activation.⁸⁷ The inhibition is achieved by targeting the dimerization interface using peptides promoting dissociation.⁸⁸ The design of small molecules intended to disrupt the dimer and /or bind to an inactive protein monomer, therefore, offers an alternative to the strategy of targeting of the active site.

In our search for MIA inhibitory compounds, we employed the HTFP assay as a rapid screening platform to identify peptides that prevent the assembly of inactive monomers to functionally active MIA dimers. The dodecapeptide AR71 was found to exhibit significant MIA inhibitory effect in *in vitro* experiments. As reflected by the HTFP assay and Western Blot analysis, inhibitory peptide AR71 promotes dissociation of MIA aggregates, while our NMR investigations revealed it to directly bind to the dimerization domain next to the distal loop.

Having demonstrated the inhibitory effect of AR71 in the *in vitro* models, we employed an established *in vivo* metastasis assay to evaluate the capability of peptide AR71 to prevent the formation of metastasis of malignant melanoma by inhibiting MIA.⁸² In our first model, Sig-AR71-HisTag expressing B16 cell clones and the respective mock control cells were analyzed for their metastatic potential. With the addition of an N-terminal secretion sequence ensuring peptide processing into the endoplasmic reticulum, we expected subsequent binding and thus inactivation of MIA by preventing formation of functionally active protein dimers directly at the location of protein biosynthesis. In immunofluorescence studies we could observe this colocalization of MIA and AR71-HisTag in the cells. In an *in vivo* mouse model, the expression of AR71 by the stably transfected B16 cells led to a dramatic reduction in the formation of metastases compared to mock control, again reflecting the need for MIA to form dimers to reach functional activity.

Even though peptides are generally quickly degraded *in vivo* by proteases and renally cleared, we also observed a significant reduction in the formation of metastases in an *in vivo* injection

model of AR71. Again, the particularly strong reduction in the number of metastases proves the potency of AR71 to suppress the metastatic spread of melanoma cells *in vivo*.

To conclude, we have contributed to the understanding of the molecular function of MIA by *in vitro* studies which included multidimensional NMR spectroscopy. These investigations revealed that MIA is functionally active as a dimer. By specifically screening MIA-binding peptide ligands for their ability to prevent MIA dimerization, we identified dodecapeptide AR71 and demonstrate the potency of this peptide to significantly reduce the formation of metastases of murine B16 malignant melanoma cells *in vivo*. This study details the mechanism by which peptide AR71 inhibits MIA mediated metastatic spread of tumor cells and provides a novel leading structure for the design of potent therapeutics for the treatment of malignant melanoma. To overcome the drug resistance observed with current treatments, this new strategy of dimerization inhibitors may be useful for prevention or at least reduction of metastatic spread in early stages of the disease. Specifically inhibiting the formation of metastases should provide a very effective therapy since malignant melanoma is not fatal because of the primary tumor but because of organ failure due to formation of metastases. In addition, most conventional treatments still affect cancer cells as well as other fast-dividing cell types, resulting in the desire for a more targeted therapy. By targeting MIA, which is only expressed in malignant melanoma and in early-phase differentiating chondrocytes, the adverse reactions of treatment with MIA inhibitory compounds should be minimal. Side effects on cartilage are not expected since MIA-deficient mice show no phenotype changes, as previously demonstrated.⁸⁹

We feel that this study provides an excellent starting point for the development of a new strategy in malignant melanoma therapy. Targeting MIA leads to strongly reduced tumor cell invasion and formation of metastases and thus provides a new concept of therapeutic intervention.

2.2.4 Materials and Methods

Cell lines and cell culture conditions

The melanoma cell line Mel Im, established from a human metastatic bioptic sample (generous gift from Dr. Johnson, University of Munich, Germany) was used in all experiments. Additionally, main experiments were also conducted using the human cell line Mel Ju and the murine cell line B16, which were derived from metastases of malignant

melanoma. All cells were maintained in DMEM (PAA Laboratories GmbH, Cölbe, Germany) supplemented with penicillin (400 U/mL), streptomycin (50 µg/mL), l-glutamine (300 µg/mL) and 10% fetal calf serum (Pan Biotech GmbH, Aidenbach, Germany) and split in a 1:6 ratio every 3 days.

Protein analysis *in vitro* (Western blotting)

Protein samples were denaturated at 70°C for 10 min after addition of reducing and denaturing Roti-Load buffer (Roth, Karlsruhe, Germany) and subsequently separated on sodium dodecyl sulfate 12.75% polyacrylamid gels (SDS-PAGE) (Invitrogen, Groningen, The Netherlands). In the multimerization studies, MIA protein (1 µg) was incubated with AR71 (2.5 µg) overnight at RT before being treated as described above. After transferring the proteins onto a polyvinylidene fluoride (PVDF) membrane (BioRad, Richmond, VA, USA), the membrane was blocked using 3% BSA/PBS for 1 h at RT and incubated with a 1:150 dilution of primary polyclonal rabbit anti MIA antibody (Biogenes, Berlin, Germany) in 3% BSA/PBS overnight at 4°C. After washing in PBS the membrane was incubated with a 1:2000 dilution of an alkaline-phosphatase coupled secondary antibody (Chemikon, Hofheim, Germany) for 2 h at RT. Finally, after washing steps, immunoreactions were visualized by nitro blue tetrazolium/5-bromo-4-chloro-3-indolyl phosphate (NBT/BCIP) (Invitrogen, Karlsruhe, Germany) staining.

Boyden Chamber Invasion Assay

Invasion assays were performed in Boyden Chambers containing polycarbonate filters with 8-µm pore size (Neuro Probe, Gaithersburg, MD, USA) essentially as described previously.⁶⁹ Filters were coated with matrigel, a commercially available reconstituted basement membrane (diluted 1:3 in H₂O; BD Bioscience, Bradford, MA, USA). The lower compartment was filled with fibroblast-conditioned medium used as a chemo attractant. Mel Im melanoma cells were harvested by trypsinization for 2 min at RT, resuspended in DMEM without FCS at a density 2.5×10^4 cells/mL, and placed in the upper compartment of the chamber. Except for the control experiment with untreated cells and experiments where cells were only treated with the respective peptide, MIA was added to the cell suspension at a final concentration of 200 ng/mL. Peptide AR71 (sequence: Ac-FHWRYPLPLPGQ-NH₂) was used at a final concentration of 1 µM. MIA expressing murine B16 melanoma cells stably co-transfected with Sig-AR71-HisTag containing pCMX-PL1 vector⁹⁰ and an antibiotic resistance comprising plasmid (pCDNA3), and the respective mock control were also investigated for

their ability to migrate. Therefore, cells were harvested by trypsinization for 2 min at RT, resuspended in DMEM without FCS at a density 2.5×10^4 cells/mL, and placed in the upper compartment of the chamber. After incubation at 37°C for 4 h filters were removed. Cells adhering to the lower surface of the filter were fixed, stained, and counted. Experiments were carried out in triplicates and repeated at least three times.

Coating of well plates with MIA-biotin

Black, streptavidin coated 96 well plates (from Greiner Bio-one, Frickenhausen, Germany) were coated with MIA-biotin as described previously.^{59, 79} An uncoated control lane was sealed with adhesive film to prevent contamination. The MIA-biotin coated plate was used for measurements immediately.

Polarization assay setup

All measurements were performed at RT on a Polarstar Optima microplate reader (BMG Labtech, Offenburg, Germany). A 390-10 nm bandpass filter was used for excitation while a 520 nm longpass filter was used for the emission light. Even though the extinction coefficient is higher at longer wavelengths, we chose a shorter excitation wavelength as this led to higher polarization values. MIA-Ru(bpy)₃ was prepared and tested for functional activity as described previously.⁷⁹ A MIA-Ru(bpy)₃ concentration of 55 fM was used in all experiments. A solution volume of 250 µL per well was found to give a low standard deviation with high signal intensity. All measurements were performed in DPBS without calcium or magnesium (PAN Biotech GmbH, Aidenbach, Germany). Addition of components to the wells was done in the following order: inhibitory peptide, buffer, MIA-Ru(bpy)₃. Owing to different reaction kinetics, measurements were performed every 5 min over a 30 min period. Polarization values are reported relative (P/P₀) to the value of free MIA-Ru(bpy)₃ in solution in a well not treated with MIA-biotin. All reported values are an average of three independent measurements.

Cloning Strategy

Signal-AR71-HisTag pCMX-PL1-plasmid construction: The Signal-AR71-HisTag pCMX-PL1 expression plasmid was created by PCR amplification of the human hydrophobic signal-peptide sequence, responsible for transport into the endoplasmic reticulum, from a Signal-MIA containing expression plasmid using the MJ Research PTC-200 Peltier Thermo Cycler (BioRad, Munich, Germany). The HisTag sequence was inserted at the C-terminal end of the AR71 peptide using the primers 5'- GAC GAA TTC ATG GCC CGG TCC CTG GTG - 3'

and 5'- GAC AAG CTT TCA GTG ATG GTG ATG GTG ATG CTG GCC GGG CAA GGG CAA GGG GTA TCT CCA GTG GAA CCT GAC ACC AGG TCC GGA GAA -3'. After amplification of the Signal-AR71-HisTag fragment, the PCR product was digested with EcoRI and HindIII (NEB, Frankfurt, Germany). The insert was purified by gel extraction (Qiagen, Hilden, Germany) and cloned into the EcoRI and HindIII sites of the eukaryotic expression vector pCMX-PL1 which was previously purified and prepared for ligation using T4-Ligase (NEB, Frankfurt, Germany).⁹⁰ After transformation in DH10 β cells (NEB, Frankfurt, Germany) according to the manufacturer's instructions, the plasmid was isolated using the MIDI Kit (Qiagen, Hilden, Germany) and quantified by a gene quant II RNA/DNA Calculator (Pharmacia Biotech, Nümbrecht, Germany). The sequence of the PCR-generated clone was confirmed by DNA sequencing.

Stable transfection of murine B16 melanoma cells

For transfection, 1.5×10^5 cells/mL were seeded in 6-well plates (Corning Omnilab, Munich, Germany) and cultured in 2 mL of Dulbecco's modified Eagle's medium (PAA, Cölbe, Germany) with 10% fetal calf serum (Pan, Aidenbach, Germany). Cells were transfected with 0.8 μ g of the respective control or His-tagged AR71 containing pCMX-PL1 vector and 0.2 μ g pcDNA3 providing geneticin (Invitrogen, Karlsruhe, Germany) resistance using the LipofectaminPlus (Invitrogen, Karlsruhe, Germany) method according to the manufacturer's instructions. After selection of cells comprising antibiotic resistance we confirmed expression and localization of AR71 peptide on mRNA and protein level by PCR and immunofluorescence, respectively.

Recombinant expression of MIA and mutant forms

In vitro protein expression reactions of recombinant human MIA and its mutants were performed with the Rapid Translation System RTS 500 E. coli HY Disulfite Kit (Roche, Mannheim, Germany) according to the manufacturer's instructions. All reactions were carried out over night at 30°C or 25°C with efficient stirring in the RTS 500 instrument. MIA mutants were checked for correct folding and function as previously described.⁶⁹

NMR Spectroscopy

All spectra were recorded at 300 K and pH 7 on a Bruker DRX600 spectrometer equipped with a pulsed field gradient triple resonance probe. Water suppression in experiments recorded on samples in H₂O was achieved by incorporation of a Watergate sequence into the

various pulse sequences.^{91, 92, 93} 2D ¹H-¹⁵N HSQC spectra with reduced signal loss due to fast exchanging protons were recorded using procedures described previously.⁹⁴ All spectra were processed with NMRPipe and analyzed with NMRView.^{95, 96} Data handling was performed with NMRView. Structure visualisation and superimpositions were done with PyMol (Delano, W. L., The PyMol Molecular Graphics System (2002) Delano Scientific, Palo Alto, CA, USA).

Dimer model

The PreBI modelling software (<http://pre-s.protein.osaka-u.ac.jp/prebi/>) was used together with the published X-ray structure of MIA (PDBid: 1I1J) for the prediction of the putative dimer interface. Employing the monomeric NMR structure of MIA (PDBid: 1HJD) together with the interface information obtained in the previous step a three-dimensional model of the dimeric complex was calculated. Computations were performed using the data driven protein-protein docking program HADDOCK.⁷⁸

Protein binding studies

The NMR titration of MIA with AR71 consisted of monitoring changes in chemical shifts and line widths of the backbone amide resonances of uniformly ¹⁵N-enriched MIA samples as a function of ligand concentration.^{97, 98, 99, 100}

***In vivo* metastasis assay**

To determine the effect of peptide AR71 on the metastatic potential of murine B16 melanoma cells *in vivo*, a previously developed mouse metastases model was used.⁸² 1×10^5 cells of the AR71-HisTag expressing B16 cell clone AR71-His K4 as well as the corresponding mock control cells were injected into the spleen of mice ($n = 8$ for mock control cells as well as for AR71-HisTag K4 cells, respectively). After nine days, mice were sacrificed, the livers were resected and the number and size of visible black tumor nodules on the surface of the livers were noticed. Tissues were fixed in formalin and afterwards paraffin embedded sections were hematoxylin and eosin stained for histological analysis.

Additionally, 1×10^5 wt mouse melanoma B16 cells suspended in a solution containing AR71 (1 mg/mL) and 0.9% NaCl, or NaCl alone for the control mice, respectively, were injected into the spleen of each animal ($n = 8$ for treated mice, as well as for control without AR71). Peptide AR71 was injected *i.v.* (50 μ g every 24 h). After nine days, the mice were sacrificed and the livers were excised. Following formalin fixation, tissues were embedded in paraffin.

Afterwards, sections were prepared and stained using hematoxylin and eosin before being subjected to histological analysis.

Immunofluorescence assays

5×10^5 murine B16 melanoma cells were grown in a 4-well chamber slide (Falcon, BD Bioscience, Heidelberg, Germany). After stable transfection with a Sig-AR71-HisTag containing expression plasmid and the respective pCMX-PL1 mock control, cells were incubated for 48 h at 37°C and 8% CO₂. Afterwards, cells were washed and fixed using 4% paraformaldehyde in 0.1 M phosphate-buffered saline (PBS) for 15 min. After permeabilization of cells, blocking of non-specific binding sites with blocking solution (1% BSA/PBS) for 1 h at 4°C was performed. Cells were incubated with primary antibodies rabbit anti-MIA (Biogenes, Berlin, Germany) and mouse anti-HisTag (BD Bioscience, Pharmingen, Germany) at a concentration of 1 µg/mL at 4°C for 2 h. After rinsing with PBS five times, cells were first covered with a 1:200 dilution of the secondary antibody TRITC anti-mouse (TRITC-conjugated donkey anti-mouse antibody, Jackson Immuno Research Laboratories, West Grove, PA, USA) and FITC anti-rabbit (FITC-conjugated polyclonal swine anti rabbit immunoglobulin, DakoCytomation, Glostrup, Denmark) in PBS at 4°C for 1 h, respectively. Following incubation with primary antibodies, cells were washed with PBS and coverslips were mounted on slides using Hard Set Mounting Medium with DAPI (Vectashield, H-1500, Linearis, Wertheim Germany) and imaged using an Axio Imager Zeiss Z1 fluorescence microscope (Axiovision Rel. 4.6.3) equipped with an Axio Cam MR camera. Images were taken using 63x oil immersion lenses.

Statistical analysis

In the bar graphs, results are expressed as mean \pm S.D. (range) or percent. Comparison between groups was made using the Student's unpaired t-test. A p-value <0.05 was considered as statistically significant (ns: not significant, *: p<0.05, **: p<0.01, ***: p<0.001). All calculations were made using the GraphPad Prism Software (GraphPad Software, Inc., San Diego, USA).

3. Summary in English and in German

English

The first part of this thesis describes the use of artificial metal chelate receptors for the recognition of phosphorylated peptides and proteins. Ditopic receptors were used for the differentiation of phosphorylated peptides in solution. After observing binding of a bis-Zn(II)-cyclen triazine to phosphorylated amino acids in a peptide in this project, new receptors were synthesized with the binding moiety coupled to a fluorophore. These compounds were then established for the detection of protein phosphorylation on SDS-PAGE.

The second part of this thesis describes a novel fluorescence polarization assay for investigating interactions of proteins with other proteins or small molecules. This assay significantly increases the molecular weight of the interaction partner which can be observed with traditional polarization assays using organic fluorophores by using a luminescent transition metal label and a functionalized wellplate as an interaction partner. In addition, a peptide deduced from this assay as inhibiting MIA (melanoma inhibitory activity) protein was found to inhibit the formation of metastases of malignant melanoma *in vivo* by belonging to a new class of cancer treatment agents, the anti metastatic agents.

German

Der erste Teil dieser Arbeit beschreibt die Verwendung von bis-Zn(II)-Cyclen Triazin Komplexen zur molekularen Erkennung von phosphorylierten Peptiden und Proteinen. Rezeptoren mit zwei Bindungsstellen wurden verwendet um phosphorylierte Peptide in Lösung zu unterscheiden. Ausgehend von diesen Ergebnissen wurden Fluoreszenz-markierte Metall Chelate zur Detektion von phosphorylierten Proteinen in der SDS-PAGE etabliert.

Der zweite Teil dieser Arbeit beschreibt einen neuartigen Fluoreszenzpolarisations Assay für die Beobachtung von Protein Wechselwirkungen. Im Gegensatz zu herkömmlichen Polarisations Assays mit organischen Fluorophoren wurde hier durch die Verwendung einer lumineszenten Übergangsmetall Chelat Markierung und einer funktionalisierten Wellplate das Spektrum der Molekularmasse des Wechselwirkungspartners erheblich erweitert. Ein mit diesem Assay gefundener Inhibitor für das MIA (melanoma inhibitory activity) Protein konnte zudem als erster Inhibitor für die Metastasierung des malignen Melanoms *in vivo* demonstriert werden und stellt damit eine gezielt anti-metastatische Tumorbehandlung dar.

4. Abbreviations

Ac acetyl

AcOH acetic acid

BCIP 5-bromo-4-chloro-3-indolyl phosphate

Boc tert-butyloxycarbonyl

BSA bovine serum albumin

DCM dichloromethane

CBB coomassie brilliant blue

Chk2 checkpoint kinase 2

DIC *N,N'*-diisopropylcarbodiimide

DIPEA diisopropylethylamine

DLS dynamic light scattering

DMEM Dulbecco's modified eagle medium

DMF *N,N*-dimethylformamide

DMSO dimethyl sulfoxide

DPBS Dulbecco's phosphate buffered saline

ECM extracellular matrix

EDTA ethylenediamine tetraacetic acid

EGTA ethyleneglycol tetraacetic acid

ELISA enzyme-linked immunosorbent assay

ESI electrospray ionization

FCS fetal calf serum

FHA forkhead associated domain

Flu fluorescein

Fmoc fluorenyl-9-methoxycarbonyl

FP fluorescence polarization

FRET fluorescence resonance energy transfer

HBTU *O*-(1-benzotriazolyl)-*N,N,N,N'*-tetramethyluronium hexafluorophosphate

HEPES 4-(2-hydroxyethyl)-1-piperazineethanesulfonic acid

HOBt hydroxybenzotriazole

HTFP heterogeneous transition metal-based fluorescence polarization

ITC isothermal titration calorimetry
kDa kilo Dalton
MeOH methanol
MIA melanoma inhibitory activity
MS mass spectrometry
MW molecular weight
NBT nitro blue tetrazolium
NMP N-methyl-2-pyrrolidone
NMR nuclear magnetic resonance
NTA nitrilo triacetic acid
PBS phosphate buffered saline
PCR polymerase chain reaction
Pin1 peptidyl-prolyl cis/trans isomerase (never in mitosis gene a)-interacting 1
PPase phosphatase
PVDF polyvinylidene fluoride
RT room temperature
Ru(bpy)₃ tris(2,2'-bipyridine) ruthenium (II)
SDS-PAGE sodium dodecyl sulfate polyacrylamide gel electrophoresis
SH2 sarcoma homology 2
SPPS solid-phase peptide synthesis
STAT signal transducer and activator of transcription
TBTU O-(benzotriazol-1-yl)- N,N,N',N'-tetramethyluronium tetrafluoroborate
TFA trifluoroacetic acid
TIS triisopropylsilane
TRIS tris(hydroxymethyl) aminomethane
Trt trityl
UV ultraviolet

5. Publications, patents and award

Publications

Schmidt, J., Riechers, A., Stoll, R., Amann, T., Fink, F., Hellerbrand, C., Gronwald, W., König, B., Bosserhoff, A. K. Dissociation of functionally active MIA protein dimers by dodecapeptide AR71 strongly reduces formation of metastases in malignant melanoma. *Nat. Med.* **2010**, (submitted).

Riechers, A., Schmidt, J., König, B., Bosserhoff, A. K. Heterogeneous Transition Metal-based Fluorescence Polarization (HTFP) Assay for Probing Protein Interactions. *Biotechniques* **2009**, *47*, 837 – 844.

Riechers, A., Grauer, A., Ritter, S., Sperl, B., Berg, T., König, B. Binding of phosphorylated peptides and inhibition of their interaction with disease-relevant human proteins by synthetic metal-chelate receptors. *J. Mol. Recognit.* **2009**, (in print).

Riechers, A., Schmidt, F., Stadlbauer, S., König, B. Detection of protein phosphorylation on SDS-PAGE using probes with a phosphate-sensitive emission response. *Bioconj. Chem.* **2009**, *20*, 804 – 807.

Grauer, A., Riechers, A., Ritter, S., König, B. Synthetic Receptors for the Differentiation of Phosphorylated Peptides with Nanomolar Affinities. *Chem. Eur. J.* **2008**, *14*, 8922 – 8927.

Hilgers, P., Riechers, A., König, B. Intelligent Materials (book recension). *Angew. Chem. Int. Ed.* **2008**, *47*, 3088 – 3089.

Kiewitz, S. D., Kruppa, M., Riechers, A., König, B., Cabrele, C. Recognition of the Helix-Loop-Helix Domain of the Id Proteins by an Artificial Luminescent Metal Complex Receptor. *J. Mol. Recognit.* **2008**, *21*, 79 – 88.

Stadlbauer, S., Riechers, A., Späth, A., König, B. Utilizing Reversible Copper(II) Peptide Coordination in a Sequence Selective Luminescent Receptor. *Chem. Eur. J.* **2008**, *14*, 2536 – 2541.

Patents

Riechers, A., Schmidt, F., Stadlbauer, S., König, B. Fluorophor compounds and methods of using the same. **2009**, EP 09 155 910.4

Bosserhoff, A. K., König, B., Schmidt, J., Riechers, A. A peptide which binds to melanoma inhibitory activity (MIA) protein. **2010**

Award

Roche Younger Investigator Award, Iceland, **2009**

6. Curriculum Vitae

Personal details

Name: Alexander Riechers
Date of Birth: July 17th, 1982
Place of Birth: Göttingen, Germany
Nationality: German
Status: Single

Education

09/2007 – present	PhD studies at the Institute of Organic Chemistry in the group of Prof. Dr. Burkhard König and at the Institute of Pathology in the group of Prof. Dr. Anja Katrin Bosserhoff, University of Regensburg, Germany. Title: Recognition of peptide and protein phosphorylation and inhibition of melanoma inhibitory activity (MIA) protein
01/2007 – 08/2007	Diploma thesis at the Institute of Organic Chemistry in the group of Prof. Dr. Burkhard König, University of Regensburg, Germany. Title: Towards sequence-specific peptide recognition – Synthesis of a combinatorial peptide library and phosphorylated peptides
10/2002 – 12/2006	Chemistry studies, University of Regensburg, Germany
09/1993 – 07/2002	Grammar school, Luitpold-Gymnasium, Wasserburg a. Inn, Germany

7. Literature

-
- ¹ Hunter, T. *Cell* **1995**, *80*, 225-236.
- ² Hunter, T. *Cell* **2000**, *100*, 113-127.
- ³ Schust, J., Sperl, B., Hollis, A., Mayer, T. U., Berg, T. *Chem. Biol.* **2006**, *13*, 1235-1242.
- ⁴ Babine, R. E., Abdel-Meguid, S. S., Mannhold, R., Kubinyi, H., Folkers, G. *Protein Crystallography in Drug Discovery*, Wiley-VCH, Weinheim, Germany, **2004**.
- ⁵ Xu, L., Chong, Y., Hwang, I., D'Onofrio, A., Amore, K., Beardley, G. P., Li, C., Olson, A. J., Boger, D. L., Wilson, I. A. *J. Biol. Chem.* **2007**, *282*, 13033-13046.
- ⁶ Kruppa, M., König, B. *Chem. Rev.* **2006**, *106*, 3520-3560.
- ⁷ Vomasta, D., Högner, C., Branda, N. R., König, B. *Angew. Chem. Int. Ed.* **2008**, *47*, 7644-7647.
- ⁸ (a) Banerjee, A. L., Eiler, D., Roy, B. C. Jia, X., Haldar, M. K., Mallik, S., Srivastava, D. K. *Biochemistry* **2005**, *44*, 3211-3224. (b) Ojida, A., Inoue, M., Mito-oka, Y., Tsutsumi, H., Sada, K., Hamachi, I. *J. Am. Chem. Soc.* **2006**, *128*, 2052-2058.
- ⁹ Manning, G., Whyte, D. B., Martinez, R., Hunter, T., Sudarsanam, S. *Science* **2002**, *298*, 1912-1934.
- ¹⁰ Manning, G., Plowman, G. D., Hunter, T., Sudarsanam, S. *Trends Biochem. Sci.* **2002**, *27*, 514-520.
- ¹¹ (a) Pandey, A., Fernandez, M. M., Steen, H., Blagoev, B., Nielsen, M. M., Roche, S., Mann, M., Lodish, H. F. *J. Biol. Chem.* **2000**, *275*, 39633-38639. (b) Pandey, A., Podtelejnikov, A. V., Blagoev, B., Bustelo, X. R., Mann, M., Lodish, H. F. *Proc. Natl. Acad. Sci. USA* **2000**, *97*, 179-184. (c) Steen, H., Kuster, B., Fernandez, M. M., Pandey, A., Mann, M. *J. Biol. Chem.* **2002**, *277*, 1031-1039. (d) Yeung, Y. G., Wang, Y., Einstein, D. B., Lee, P. S., Stanley, E. R. *J. Biol. Chem.* **1998**, *273*, 17128-17137. (e) Machida, K. et al. *Mol. Cell* **2007**, *26*, 899-915.
- ¹² Grauer, A., Riechers, A., Ritter, S., König, B. *Chem. Eur. J.* **2008**, *14*, 8922-8927.
- ¹³ (a) Darnell Jr, J. E. *Nat. Rev. Cancer* **2002**, *2*, 740-749. (b) Schindler, C., Levy, D. E., Decker, T. *J. Biol. Chem.* **2007**, *282*, 20059-20063.
- ¹⁴ Lim, C. P., Cao, X. *Molecular BioSystems* **2006**, *2*, 536-550.
- ¹⁵ Berg, T. *ChemBioChem* **2008**, *9*, 2039-2044.
- ¹⁶ Antoni, L., Sodha, N., Collins, I., Garrett, M. D. *Nat. Rev. Cancer* **2007**, *7*, 925-936.

-
- 17 Wu, P., Brasseur, M., Schindler, U. *Anal. Biochem.* **1997**, 249, 29-36.
- 18 Li, J., Williams, B. L., Haire, L. F., Goldberg, M., Wilker, E., Durocher, D., Yaffe, M.
B., Jackson, S. P., Smerdon, S. J. *Mol. Cell.* **2002**, 9, 1045-54.
- 19 Williams, D. H., Westwell, M. S. *Chem. Soc. Rev.* **1998**, 27, 57-63.
- 20 Ojida, A., Inoue, M.A., Mito-oka, Y., Tsutsumi, H., Sada, K., Hamachi, I. *J. Am. Chem.
Soc.* **2006**, 128, 2052-2058.
- 21 Riechers, A., Grauer, A., Ritter, S., Sperl, B., Berg, T., König, B. *J. Mol. Recognit.*
2009, in press.
- 22 Pío, R., Martínez, A., Unsworth, E. J., Kowalak, J. A., Bengoechea, J. A., Zipfel, P. F.,
Elsasser, T. H., Cuttitta, F. *J. Biol. Chem.* **2001**, 276, 12292-12300.
- 23 Misenheimer, T. M., Hahr, A. J., Harms, A. C., Annis, D. S., Mosher, D. F. *J. Biol.
Chem.* **2001**, 276, 45882-45887.
- 24 Williams, N. K., Prosser, P., Liepinsh, E., Line, I., Sharipo, A., Littler, D. R.,
Curmi, P. M. G., Otting, G., Dixon, N. E. *J. Biol. Chem.* **2002**, 277, 7790-7798.
- 25 Schulenberg, B., Goodman, T. N., Aggeler, R., Capaldi, R. A., Patton, W. F. *J.
Electrophoresis* **2004**, 24, 2526-2532.
- 26 Kinoshita, E., Kinoshita-Kikuta, E., Takiyama, K., Koike, T. *Mol. Cell. Proteomics*
2006, 5, 749-757.
- 27 Manning, G., Whyte, D. B., Martinez, R., Hunter, T., Sudarsanam, S. *Science* **2002**,
298, 1912-1934.
- 28 Salomon, A. R., et al. *Proc. Natl. Acad. Sci. USA* **2003**, 100, 443-448.
- 29 Conrads, T. P., Veenstra, T. D. *Nat. Biotechnol.* **2005**, 23, 36-37.
- 30 Larsen, M. R., Sorensen, G. L., Fey, S. J., Larsen, P. M., Roepstorff, P. *Proteomics*
2001, 1, 223-238.
- 31 Immler, D., Gremm, D., Kirsch, D., Spengler, B., Presek, P., Meyer, H. E. *J.
Electrophoresis* **1998**, 19, 1015-1023.
- 32 Ojida, A., Kohira, T., Hamachi, I. *Chem. Lett.* **2004**, 33, 1024-1025.
- 33 Ojida, A., Mito-oka, Y., Inoue, M., Hamachi, I. *J. Am. Chem. Soc.* **2002**, 124, 6256-
6258.
- 34 Mizukami, S., Nagano, T., Urano, N., Odani, Y., Kikuchi, K. *J. Am. Chem. Soc.* **2002**,
124, 3920-3925.
- 35 Wolfbeis, O. S., Uray, G. *Monatsh. Chem.* **1978**, 109, 123-136.

36 To assess the influence of the fluorophore further, we also prepared the same type of
probe with pyrene and dansyl fluorophores. Neither of these probes exhibited any
distinction between phosphorylated and nonphosphorylated proteins (data not shown).
37 Kruppa, M., Frank, D., Leffler-Schuster, H., König, B. *Inorg. Chim. Acta* **2006**, 359,
1159-1168.
38 Lugina, L. N., Davidenko, N. K., Gavrish, S. P. *Theor. Exp. Chem.* **1985**, 21, 466-470.
39 Hou, J. L., Yi, H. P., Shao, X.-B., Li, C., Wu, Z.-Q., Jiang, X.-K., Wu, L.-Z., Tung, C.-
H., Li, Z.-T. *Angew. Chem.* **2004**, 117, 118-122.
40 Riechers, A., Schmidt F., Stadlbauer, S., König, B. *Bioconj. Chem.* **2009**, 20, 804-807.
41 Dürkop, A., Lehmann, F., Wolfbeis, O. S. *Anal. Bioanal. Chem.* **2002**, 372, 688-694.
42 Castellano, F.N., Guo, X. Q., Lakowicz, J. R. *Biophys. J.* **1998**, 70, 632-637.
43 Szmazinski, H., Castellano, F. N., Terpetschnig, E., Dattelbaum, J. D., Lakowicz, J. R.,
Meyer, G. J. *Biochim. Biophys. Acta* **1998**, 1383, 151-159.
44 Guo, X.Q., Castellano, F. N., Li, L., Lakowicz, J. R. *Anal. Chem.* **1998**, 70, 632-637.
45 Terpetschnig, E., Dattelbaum, J. D., Szmazinski, H., Lakowicz, J. R. *Anal. Biochem.*
1997, 251, 241-245.
46 Terpetschnig, E., Szmazinski, H., Lakowicz, J. R. *Anal. Biochem.* **1996**, 240, 54-59.
47 Szmazinski, H., Terpetschnig, E., Lakowicz, J. R. *Biophys. Chem.* **1996**, 62, 109-120.
48 Terpetsching, E., Szmazinski, H., Malak, H., Lakowicz, J. R. *Biophys. J.* **1995**, 68, 342-
350.
49 Terpetsching, E., Szmazinski, H., Lakowicz, J. R. *Anal. Biochem.* **1995**, 227, 140-147.
50 Sarwar, M., Nasir, M., Jolley, M. E. *Combinatorial Chemistry & High Throughput
Screening* **1999**, 2, 177-190.
51 Hun, X., Zhang, Z. *Talanta* **2007**, 73, 366-371.
52 Sanchez-Martinez, M.L., Aguilar-Caballos, M. P., Gomez-Hens, A. *Anal. Chem.* **2007**,
79, 7424-7430.
53 Sanchez-Martinez, M.L., Aguilar-Caballos, M. P., Eremin, S. A., Gomez-Hens, A.
Talanta **2007**, 72, 243-248.
54 Bosserhoff, A. K., Kaufmann, M., Kaluza, B., Bartke, I., Zirngibl, H., Hein, R., Stolz,
W., Buettner, R. *Cancer Res.* **1997**, 57, 3149-3153.
55 Bosserhoff, A. K., Buettner, R. *Biomaterials* **2003**, 24, 3229-3234.
56 Dreau, D., Bosserhoff, A. K., White, R. L., Buettner, R., Holder, W. D. *Oncol. Res.*
1999, 11, 55-61.

-
- 57 Stahlecker, J., Gauger, A., Bosserhoff, A. K., Buettner, R., Ring, J., Hein, R. *Anticancer Res.* **2000**, *20*, 5041-5044.
- 58 Bosserhoff, A.K., Buettner, R. *Histol. Histopathol.* **2002**, *17*, 289-300.
- 59 Bauer, R., Humphries, M., Fassler, R., Winklmeier, A., Craig, S. E., Bosserhoff, A. K. *J. Biol. Chem.* **2006**, *281*, 11669-11677.
- 60 Bosserhoff, A. K., Stoll, R., Sleeman, J. P., Bataille, F., Buettner, R., Holak, T. A. *Lab. Invest.* **2003**, *83*, 1583-1594.
- 61 Stoll, R., Renner, C., Zweckstetter, M., Bruggert, M., Ambrosius, D., Palme, S., Engh, R. A., Golob, M., Breibach, I., Buettner, R., Voelter, W., Holak, T. A. Bosserhoff, A. K. *EMBO J.* **2001**, *20*, 340-349.
- 62 Schmidt, J., Bosserhoff, A. K. *Int. J. Cancer* **2009**, *125*, 1587-1594.
- 63 Ismail, K. Z., Weber, S. G. *Biosens. Bioelectron.* **1991**, *6*, 699-705.
- 64 Myszka, D.G. *Anal. Biochem.* **2004**, *329*, 316-323.
- 65 Wu, Y., Li, Q., Chen, X. Z. *Nature Protocols* **2007**, *2*, 3278–3284.
- 66 Arany, I., Faisal, A., Nagamine, Y., Safirstein, R. L. *J. Biol. Chem.* **2008**, *283*, 6110-6117.
- 67 Gasyimov, K., Glasgow B. J. *Biochim. Biophys. Acta* **2007**, *1774*, 403-411.
- 68 Lakowicz, J. R. Principles of fluorescence spectroscopy. Springer Science + Business Media LLC, New York, **2006**.
- 69 Stoll, R., Lodermeier, S., Bosserhoff, A. K. *Biol. Chem.* **2006**, *387*, 1601-1606.
- 70 Blesch, A. et al. *Cancer Res.* **1994**, *54*, 5695-5701.
- 71 Bosserhoff, A. K., Echtenacher, B., Hein, R., Buettner, R. *Melanoma Res.* **2001**, *11*, 417-421.
- 72 Guba, M. et al. *Br. J. Cancer* **2000**, *83*, 1216-1222.
- 73 Schmidt, J., Friebel, K., Schönherr, R., Coppolino, M. G., Bosserhoff, A. K. *Int. J. Cancer* **2010**, submitted.
- 74 Stoll, R., Bosserhoff, A. *Curr. Protein Pept. Sci.* **2008**, *9*, 221-226.
- 75 Stoll, R. et al. *J. Biomol. NMR* **2000**, *17*, 87-88.
- 76 Stoll, R. et al. *Protein Sci.* **2003**, *12*, 510-519.
- 77 Loughheed, J. C., Holton, J. M., Alber, T., Bazan, J. F., Handel, T. M. *Proc. Natl. Acad. Sci. USA* **2001**, *98*, 5515-5520.
- 78 Dominguez, C., Boelens, R., Bonvin, A.M.J.J. *J. Am. Chem. Soc.* **2003**, *125*, 1731-1737.

-
- 79 Riechers, A., Schmidt, J., König, B., Bosserhoff, A. K. *Biotechniques* **2009**, 47, 837-844.
- 80 Bosserhoff, A. K., Hein, R., Bogdahn, U., Buettner, R. *J. Biol. Chem.* **1996**, 271, 490-495.
- 81 Bosserhoff, A. K. et al. *Anticancer Res* **1999**, 19, 2691-2693.
- 82 Carrascal, M. T. et al. *Cancer Res.* **2003**, 63, 491-497.
- 83 Lougheed, J. C., Domaille, P. J., Handel, T. M. *J. Biomol. NMR* **2002**, 22, 211-223.
- 84 Osborne, J. C., Jr., Bengtsson-Olivecrona, G., Lee, N. S., Olivecrona, T. *Biochemistry* **1985**, 24, 5606-5611.
- 85 Nomura, A. M., Marnett, A. B., Shimba, N., Dotsch, V., Craik, C. S. *Biochemistry* **2006**, 45, 3572-3579.
- 86 Pray, T. R., Nomura, A. M., Pennington, M. W., Craik, C. S. *J. Mol. Biol.* **1999**, 289, 197-203.
- 87 Wlodawer, A. et al. *Science* **1989**, 245, 616-621.
- 88 Boggetto, N., Reboud-Ravaux, M. *Biol. Chem.* **2002**, 383, 1321-1324.
- 89 Moser, M. et al. *Mol. Cell. Biol.* **2002**, 22, 1438-1445.
- 90 Tatzel, J., Poser, I., Schroeder, J., Bosserhoff, A. K. *Pigment Cell. Res.* **2005**, 18, 92-101.
- 91 Braunschweiler, L., Ernst, R. R. *J. Magn. Reson.* **1983**, 53, 521-528.
- 92 Davis, D. G., Bax, A. *J. Am. Chem. Soc.* **1985**, 107, 7197-7198.
- 93 Shaka, A. J., Lee, C. J., Pines, A. *J. Magn. Reson.* **1988**, 77, 274-293.
- 94 Mori, S., Abeygunawardana, C., Johnson, M. O., van Zijl, P. C. *J. Magn. Reson. B* **1995**, 108, 94-98.
- 95 Johnson, R. D., Bluemler, P., Rafey, R., Brodbeck, D. *Abstr. Pap. Am. Chem. S.* **1994**, 207.
- 96 Delaglio, F. et al. *J. Biomol. NMR* **1995**, 6, 277-293.
- 97 Berghaus, C., Schwarten, M., Heumann, R., Stoll, R. *Biomol. NMR Assign.* **2007**, 1, 45-47.
- 98 Schwarten, M., Berghaus, C., Heumann, R., Stoll, R. *Biomol. NMR Assign.* **2007**, 1, 105-108.
- 99 Song, J., Markley, J. L. *J. Mol. Recognit.* **2001**, 14, 166-171.
- 100 Stoll, R. et al. *Biochemistry* **2001**, 40, 336-344.